CHALMERS

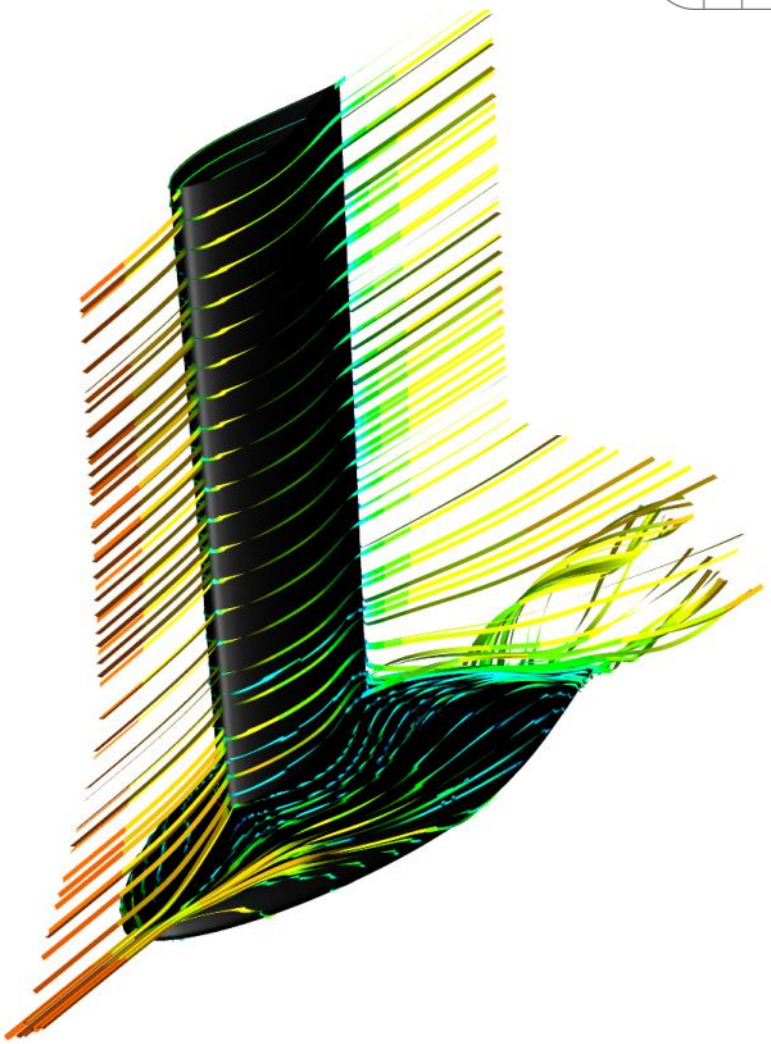

Investigation of Keel Bulbs for Sailing Yachts

Master of Science Thesis

BJÖRN AXFORS
HANNA TUNANDER

Department of Shipping and Marine Technology
Marine Hydrodynamics
CHALMERS UNIVERSITY OF TECHNOLOGY
Göteborg, Sweden, 2011
Report No. X-11/263

A THESIS FOR THE DEGREE OF MASTER OF SCIENCE

Investigation of Keel Bulbs for Sailing Yachts

BJÖRN AXFORS

HANNA TUNANDER

Department of Shipping and Marine Technology

Marine Hydrodynamics

CHALMERS UNIVERSITY OF TECHNOLOGY

Gothenburg, Sweden 2011

Investigation of Keel Bulbs for Sailing Yachts

BJÖRN AXFORS
HANNA TUNANDER

Master's Thesis X-11/263
Department of Shipping and Marine Technology
Chalmers University of Technology
SE-412 96 Gothenburg
Sweden
Telephone +46 (0)31-772 1000

Printed by Chalmers Reproservice
Gothenburg, Sweden, 2011

Investigation of Keels Bulbs for Sailing Yachts

BJÖRN AXFORS
HANNA TUNANDER
Department of Shipping and Marine Technology
Marine Hydrodynamics
Chalmers University of Technology

Abstract

In this master's thesis an evaluation of the performance of four different keel designs has been made. The keels were designed for a performance pleasure sailing yacht, more specifically the YD-40 which is a 40 foot sailing yacht from Principles of Yacht Design [1].

The designs are: a fin keel, an integrated L-bulb keel, an L-bulb keel and a T-bulb keel. All design types can be found on existing sailing yachts but there has been little research made which clearly explains why one should be chosen before another from a hydrodynamic point of view.

The evaluation of the performance of the four different designs has been made both by using RANS (Reynolds Averaged Navier Stokes) CFD (Computational Fluid Dynamics) as well as wind tunnel testing of keel models. Force coefficients and force trends were measured in the wind tunnel were then compared with the coefficients gained from CFD.

More quantitative results are also presented which were derived using VPP (Velocity Prediction Program), calculating the race time for an Olympic race course of the keels together with hull.

One important additional purpose of the thesis was to contribute to an open information platform of wind tunnel results for validating CFD; most existing work in this field has been made by professional sailing teams, and since this involves investments of huge amounts of time and effort the results are rarely open for the public.

Keywords: Sailing Yacht, Bulb, Keel, Wind tunnel, Verification, CFD, Validation, VPP

Sammanfattning

I detta examensarbete har en utvärdering av prestandan för fyra olika kölprofiler genomförts. Kölarna är designade för fritidssegelbåtenYD-40, en 40 fots segelbåt från boken Principles of Yacht Design [1].

De olika designerna är: en fenköl, en integrerad L-bulb köl, en L-bulb köl och en T-bulb köl. Alla dessa designtyper kan hittas på befintliga segelbåtar idag, men det har gjorts väldigt lite forskning som tydligt förklarar varför man bör välja den ena designen framför en annan utifrån en hydrodynamisk synvinkel.

Utvärderingen av de fyra olika kölarna har gjorts både med hjälp av RANS simuleringar i CFD samt med vindtunneltest. Kraftkoefficienter mätta i vindtunneln har jämförts med de koefficienter som beräknats i CFD.

Ett VPP program har använd för att jämföra hur de olika kölarna, tillsammans med ett skrov, presterar på ett race. En OS-bana har används för att ranka de olika kölarna mot varandra.

Ytterligare ett viktigt syfte med avhandlingen var att bidra till en öppen informationsplattform av CFD resultat som validerats med en vindtunnel. De flesta befintliga insatser på detta område har gjorts av professionella seglingsteam och eftersom detta ofta innebär enorma investeringar både vad gäller pengar och tid så är resultaten sällan öppna för allmänheten.

Nyckelord: Segelbåt, Köl, Bulb, Vindtunnel, Verifiering, CFD, Validering, VPP

Acknowledgements

This Master's Thesis was made possible by the respected and well known enthusiast within yacht design, Prof. Lars Larsson. We owe him for giving us this opportunity, and also for his endless interests in our tasks and his expert help along the way.

We would like to express our gratitude to our supervisor Michał Orych, who supported us throughout the whole project, and whose knowledge in SHIPFLOW was crucial for reaching useful results.

Florian Vesting's help was very valuable for us in the first stage of the project in the redesign of the T-keel, and we owe him for this.

Prof. Rickard Bensow helped us with file conversions for the CFD which speeded up our work.

We would also thank the crew of the wind tunnel at applied mechanics for their cooperation during the testing, and also their flexibility regarding the planning of the testing dates.

For support and discussion about SHIPFLOW we would like to thank Björn Regnström, and we hope we have given him some interesting feedback for further development of the software.

We also would like to thank Kasper Ljungqvist both for exchanging ideas during the thesis, as well as for valuable feedback on the report.

We would also like to mention the designer of Arcona Yachts, Stefan Qviberg, who together with Prof. Larsson was behind the idea of the thesis.

Last but not least we would like to thank Lotta Olsson on the administration of Naval Architecture for her help not only throughout the thesis but during the whole Master's programme.

It has been most inspiring working with our experienced examiner and supervisor to contribute to the development of sailing yachts.

Göteborg, 2011-06-10

Björn Axfors

Hanna Tunander

Table of Contents

Nomenclature

ADI	Alternating Directions Implicit
A_L	Lateral area
ANSYS ICEM	Software used for meshing
AoA	Angle of Attack
AR	Aspect Ratio
CAD	Computer Aided Design
C_D	Drag coefficient
C_{DI}	Drag coefficient for induced drag
C_{DP}	Drag coefficient for viscous (parasitic) drag
C_f	Skin friction coefficient
CFD	Computational Fluid Dynamics
C_L	Lift Coefficient
$C_{L,Prandtl}$	Lift coefficient according to Prandtl's formula
$C_{L,WF}$	Lift coefficient according to Whicker and Fehlner's formula
CNC	Computer Numerical Control
C_P	Pressure coefficient
D	Drag Force
EASM	Explicit Algebraic Stress Model
JAVAFOIL	Internet based software for 2-D foils
L	Lift Force
LES	Large Eddy Simulation
lfib1	The total velocity vector
NACA	National Advisory Committee for Aeronautics
RANS	Reynolds Averaged Navier Stokes
R_n	Reynolds Number
ROE	Flux discretization method
SHIPFLOW	Software used for CFD calculations

S_W	Wetted Surface
VCG	Vertical centre of gravity
VPP	Velocity Prediction Program
XCHAP	The viscous flow solver in SHIPFLOW
YD-40	Yacht Design 40, 40 foot yacht from Principles of Yacht Design [1]

1 Introduction

In the introduction part the background to this thesis will be explained. Also the aim and objectives as defined in the early planning stage, as well as demarcations in these. Finally the methodology used throughout the thesis will be described.

1.1 Background

Yacht sailing and competition is and has always been attracting the attention both of investors and skilled scientists across the world. In recent years more and more sophisticated computational techniques have been put into use for performing the extensive researches within the field. These involve research and development in hull design, sail, appendages design and sailing strategy. In competitive sailing, as the famous Americas Cup or Volvo Ocean Race, endless amounts of money and resources are invested by the teams in optimizing the performance of the yachts. Most results and designs are confidential for the public and few can be read and further used for comparison.

There is of course a huge difference between a typical race keel and a keel designed for a pleasure sailing yacht, both in design targets and robustness, but trends in performance of different designs from the performance yachts could still be useful for the pleasure yachts.

In pleasure yachting today, sailing yachts are produced with very different keel set-ups. All keels have their certain advantages and disadvantages, but the variety of different keel design reveal very little about which set-up is the best in a performance and usefulness point of view. A specific comparison between different set-ups could be useful both for the customers, further research, the manufacturers and designers.

A bachelor's thesis was carried out in the spring 2010 on this subject [2]. Four different keel designs were compared: a fin-keel, an integrated L-keel, an L-keel and a T-keel. Demarcations were set in order to make a comparison possible. The results did however not turn out as expected. One main part that differed from what was expected was the performance of the T-keel. One possible reason for this was believed to be a severely separating flow behind the keel due to the bulb design resulting in large energy dissipation in vortices left behind in the wake. Another reason was thought to be that the CFD (Computational Fluid Dynamics) calculations were not validated, and the reliability of these was questioned. These possibilities of improvement were the starting point for this master's thesis. [2]

1.2 Aim and objectives

The aim of this project is to evaluate four different keels and determine which one has best performance upwind. One of the keels, the T-keel, will firstly be completely redesigned based on both discussions with our examiner Prof. Lars Larsson and our supervisor Michał Orych as well as conclusions drawn from the results from the bachelor's thesis.

The main approach for determining the performance will be to evaluate the keels with a RANS (Reynolds Averaged Navier Stokes) CFD program and compare and validate the resulting forces with wind tunnel testing. This comparison will also be a platform for validation of future CFD calculations. Some more quantitative values from a VPP (Velocity Prediction Program) for the keels together with the hull of the YD-40 [1] will then be calculated to present and compare the results further.

1.3 Demarcations

The four keels should have the same righting moment in order to be comparable. This means that the static moment of the yacht which counteracts side forces from the sails should be the same. In the redesign of the T-keel, this righting moment has to be kept constant. For an easy comparison between the keel designs the draft will be kept constant as well, and the fin size and shape will be identical between the bulb keels.

CFD calculations will be carried out for zero and four degrees angle of attack for all the keels. The method to be used is RANS, and no comparison with potential flow calculations or higher grade viscous solvers such as LES (Large Eddy Simulation) will be made.

In the wind tunnel testing part only the forces on the keels will be measured for the validation of the CFD results. Local pressures or flow characteristics in the wind tunnel or around the keels would not be measured due to the limited time-span in the wind tunnel.

Both the tests in the wind tunnel and the CFD calculations will be run at model scale for comparison reasons. A dimension analysis will be performed and full scale forces and performance will be presented.

Other demarcations in the evaluation in both the wind tunnel and within CFD will be as follows:

- No heel angle
- 4 keel designs
- The set-up in the CFD domain would match the wind tunnel conditions
- Forces for zero and four degrees angle of attack will be compared between CFD and wind tunnel tests

1.4 Methodology

As mentioned in the aim and demarcations of this master's thesis, the methodology has involved two main approaches for the evaluation of the performance of the keels: RANS CFD and wind tunnel testing. The results have been compared and are presented in the thesis. More quantitative comparative results have also been gained using VPP. For the re-design work of the T-keel a CAD (Computational Aided Design) program has been used. In Figure 1 the global structure of the methodology is illustrated.

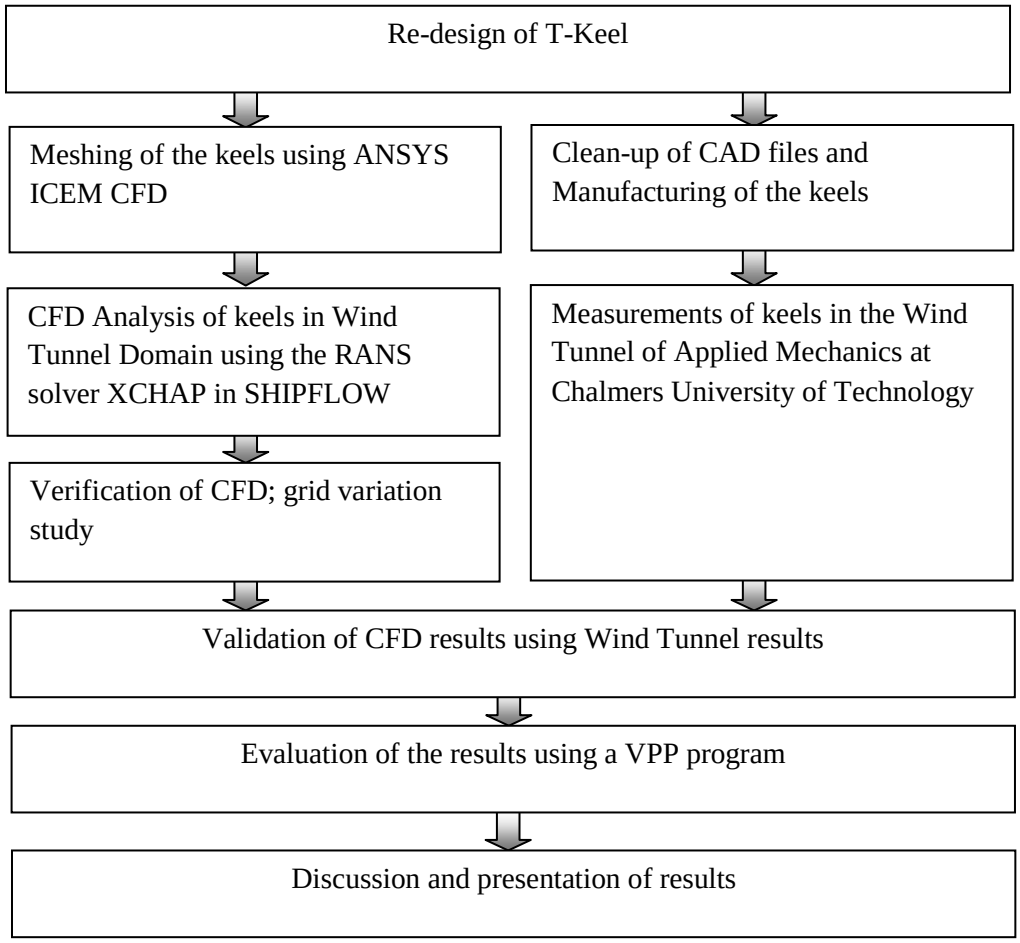

Figure 1: Methodology

2 The Keels

The basic keel designs which have been investigated in this master's thesis were taken from a previous bachelor's project that was carried out in the spring 2010 [2]. For comparison reasons the keels have equal righting moment and maximum draft. There are four different designs with the corresponding numbering which we will use throughout the report:

- Keel 1 / K1: Fin-keel
- Keel 2 / K2: Integrated L-keel
- Keel 3 / K3: L-bulb keel
- Keel 4 / K4: T-bulb keel

Keel 1 was used only as a comparison for the other keels. It does have the same righting moment and maximum draft, but in order to fulfil this it had to be designed to be made of lead instead of cast iron as the other keels. This implies it will have a comparably smaller wetted surface, and consequently the drag forces will be smaller. The effects of these aspects were expected to occur in the results.

From Figure 2 it can be seen that the frictional resistance of the yacht is a major part of its total resistance. The keel also contributes to the induced resistance. These numbers corresponds to the YD-40 equipped with its original keel.

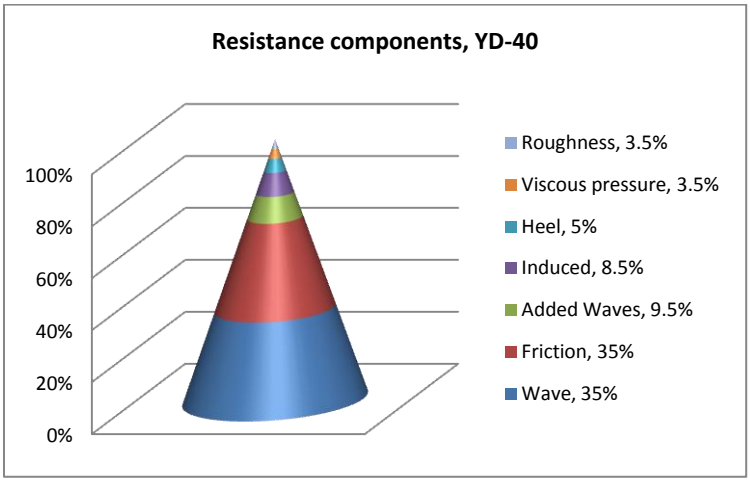

Figure 2: Resistance components, YD-40 beating to windward at 6.8 knots [1]

2.1 General design aspects

The purpose of the keel is twofold: to balance the side force from the sails and to increase the righting moment which balances the heeling moment due to the sail forces. The forces on a yacht that is sailing with constant speed are in equilibrium, the sum of all forces equal to zero. All the forces on a yacht during sailing are shown in Figure 3.

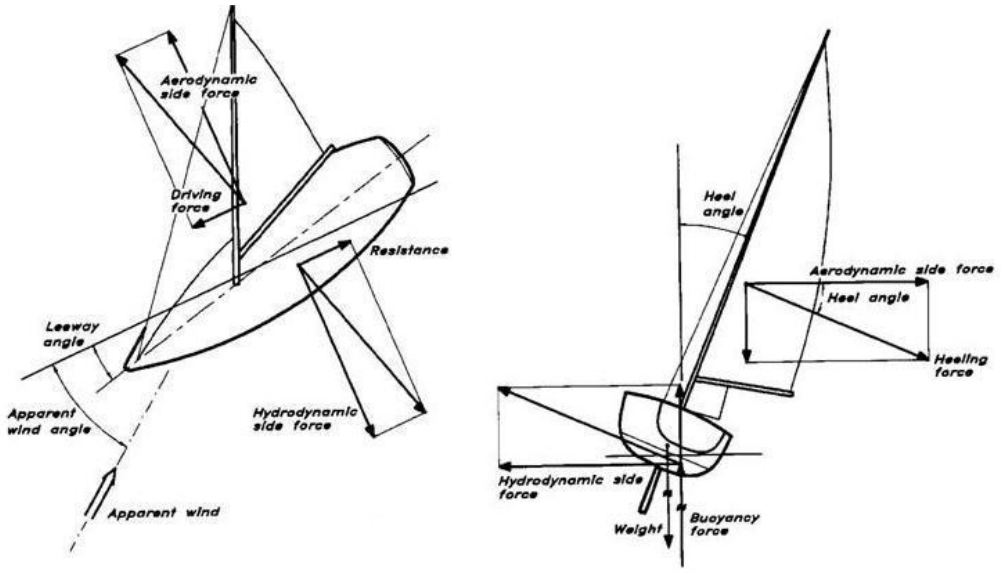

Figure 3: Forces acting on a sailing yacht, from [1] by permission by the author

The advantage with a bulb keel instead of a fin keel is that it has a significant lower vertical centre of gravity. The disadvantage is that a bulb keel usually has a lower lift to drag. The keel is always placed so that the forces on the yacht are in balance both regarding heel and trim. The benefit with the T-keel in comparison with the two other bulb keels is that the fin and the bulb can be placed independently. First the fin can be mounted on the most optimal place relative to the sail plan, i.e. where the yawing moment is balanced by a small weather helm. The bulb can then be moved to that position where the total trim for the yacht is equal to zero. For the other bulb keels there will be a compromise between the optimum places for the yawing moment and the optimum place for reducing the trim.

When designing a keel for a real yacht the keel is a part of the global design cycle of the yacht. Aspects which define the keel dimensions, design type, position and material are for example which yacht type it is to be designed for; if the yacht should be optimized for down- or upwind performance; price; materials used in the hull; wanted righting moment and maximum draft. There are several rules from classification societies to be fulfilled, which also affect the final design of the keel. [3]

In this master's thesis different keels were designed for an existing yacht design, namely the YD-40 [1]. By keeping the previously mentioned aspects constant the keels in this thesis are still reasonable for fitting to this yacht, even though they were not a part of the basic design cycle.

All keels were built up from NACA (National Advisory of Aeronautics) profiles [4]. NACA 65 and 63 series were used for all the fins in order to make these less contributing to the difference in keel performance. These NACA sections are often used for keels for their high lift to drag ratio in low angles of attack. They do however have a lower stalling angle than other sections, but since a keel operates in relative low angles of attack, this will not cause any problems. Different NACA profiles have also been used for shaping the different bulbs. More detailed descriptions can be gained by requesting the authors for the complete CAD drawings.

Both the fin-keel, the integrated L-keel and the non-integrated L-keel are virtually the same as in the bachelor's thesis. Some minor changes were made for manufacturing reasons, for example the trailing edges were cut off to a thickness of 2mm for the model scale. The T-keel was changed completely in order to increase its performance.

In the following figures the keel designs can be seen in side- and front view. In Appendix B perspective views of all keels are displayed.

Figure 4: Keel 1, fin keel

Figure 5: Keel 2, integrated L-bulb keel

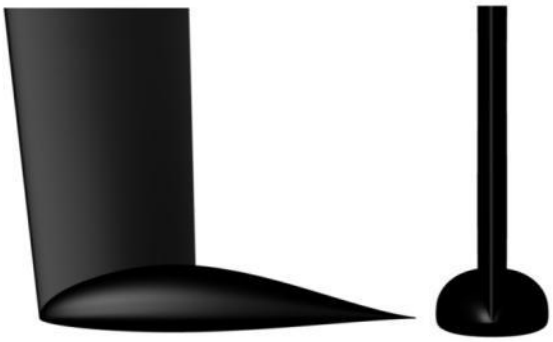

Figure 6: Keel 3, L-bulb keel

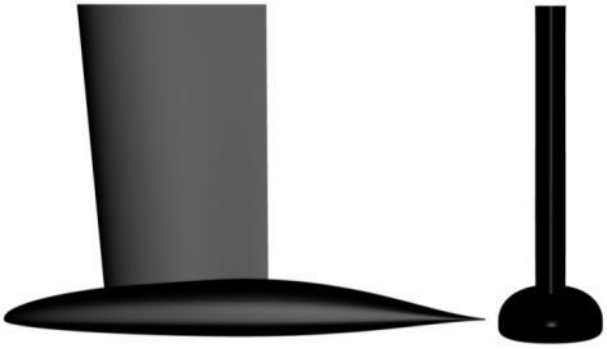

Figure 7: Keel 4, T-bulb keel

The differences between the keels in this master's thesis, which were designed for a pleasure yacht, and the keels of racing yachts are many. For example the fin on a pleasure yacht has to give sufficient lift force for manoeuvring in low speed where a fin with a shorter chord length would stall, whereas a racing yacht will only operate in higher speeds and can have short chord length on the keel to minimize the wetted surface. A T-keel is commonly found for racing yachts designed for upwind, such as Americas Cup yachts, where a lot of weight is needed in the bulb to provide large righting moment. This is mainly for practical reasons, since the fitting of other bulb types to a very long and narrow fin would be impossible.

2.2 Redesign of T-keel

For the designing of the new T-keel some aspects and constraints had to be taken into account. The reason for redesigning the keel was because of the poor behaviour the results from the bachelor's thesis showed. The large drag originated from a massive separation on the suction side of the keel, and this was caused of a poor design placing the minimum pressure zones of the keel fin and bulb on the same position in longitudinal direction.

For the design work and also for gaining some hydrostatic parameters needed to ensure the design targets and the demarcations of these were fulfilled, the CAD software in FRIENDSHIP FRAMEWORK SYSTEMS was used.

It was concluded from discussions with our examiner Prof. Lars Larsson and supervisor Michał Orych that the most important design target was to reduce the separation. In order to achieve this it was considered important that the pressure minimum on the bulb was moved as far away as possible from the pressure minimum of the fin. The bulb was there for designed with its maximum thickness, both vertically and sideward, at the trailing edge of the fin. The bulb was also designed to push the flow and trailing vortices downward in order to gain an induced draft change which could be beneficial for the performance of the yacht.

NACA 65017 is used for the side profile. This is a NACA section of series 6, with pressure minimum at 50% chord length and with a section thickness 17% of the chord length. This profile was then scaled to a larger size and cut off to create a beaver-tail on the bulb. Beaver-tails are often seen in existing designs, and the main purpose of these is to make the flow follow the shape in draft direction and possibly to push the flow down. The pressure minimum for this scaled profile occurs where the trailing edge of the fin is connected to the bulb.

To be able to have the same pressure minimum position for the bottom and top profile a combination between NACA 65 and NACA 66 series had to be used. This modified profile was created and tested using internet based software called JAVA foil [5] to ensure that the profile had the pressure minimum at the right position. It was then scaled and used for both the top and the bottom of the bulb, with the bottom section scaled to a thickness of 8% of the chord length and the top section 15%. The reasons for the flatter bottom curve is both for practical reasons – to have a stable support to place the yacht upon when on land, but also to lower the VCG as much as possible. The most important reason is to keep the trailing vortices as low as possible and hence increase the effective draft.

The design work resulted in a keel quite different compared to the old design, as can be seen in Figure 8 and Figure 9 below.

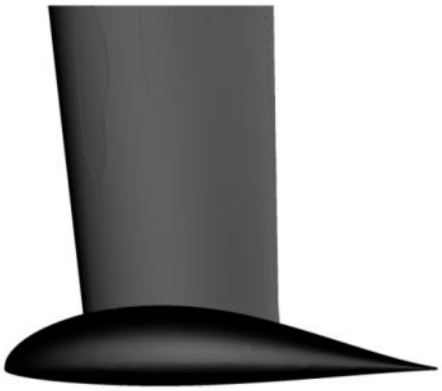

Figure 8: Old T-keel

Figure 9: New T-keel

3 Investigation of the Keels

In this part the two major techniques used in the investigation and described in the methodology will be explained. The results presented in this chapter are a comparison between the keels only. A comparison between CFD and Wind Tunnel tests is presented in the global results part on page 40.

3.1 CFD

Most CFD software is based on the incompressible three dimensional Navier-Stokes equations, with more or less assumptions for simplification. These equations balance the fluid acceleration with the pressure, body and viscous forces in the fluid. When combined with the three dimensional continuity equation, and applying the correct boundary conditions, these equations are numerically solvable [6].

It is possible to solve these equations numerically without simplification using DNS (Direct Numerical Simulation); however this is not applicable on large flow cases due to the extreme computational cost it would require. Instead the equations are split into two parts as a simplification: Potential flow theory which only takes the pressure forces into account, and viscous flow theory for the viscous effects. Furthermore, the viscous part must be further simplified for getting a reasonable computational cost.

In this thesis a RANS solver was used which is a time averaged form of the Navier Stokes equations. Solving with RANS will give the time averaged pressure and velocity, and since the fluctuating parts of these are usually of a smaller magnitude this is often seen as a good choice for evaluating flow cases. For the same reason, it was seen as a good choice for the evaluation of the keels.

The RANS methods consider the fluid velocity to consist of a constant and a fluctuating part. The fluctuating terms give rise to Reynolds stresses and are directly connected to the turbulence of the flow, and for this turbulence models have been introduced. The choice of solver and turbulence model is a crucial step towards a useful result, and every decision must be based on theory and experience to ensure that the results can be trusted.

Boundary conditions are specified for every component in the computational domain. The initial guess for these in RANS calculations are described in Table 1 where:

- u = Velocity
- u_i = Time average velocity components
- n_i = Normal to surface
- p = Pressure
- k = Turbulent kinetic energy
- ω = Specific dissipation of turbulent kinetic energy, turbulent frequency
- ξ_B = Parameter direction crossing the boundary

Table 1: Boundary conditions [7]

	Noslip	Slip	Inflow	Outflow
$\boldsymbol{u}$	$u_i = 0$	$u_i n_i = 0, \quad \frac{\partial u_i}{\partial \xi_B} = 0$	$u_i = Constant$	$\frac{\partial u_i}{\partial \xi_B} = 0$
$\boldsymbol{p}$	$\frac{\partial p}{\partial \xi_B} = 0$	$\frac{\partial p}{\partial \xi_B} = 0$	$\frac{\partial p}{\partial \xi_B} = 0$	$p = 0$
$\boldsymbol{k}$	$k = 0$	$\frac{\partial k}{\partial \xi_B} = 0$	$k = Constant$	$\frac{\partial k}{\partial \xi_B} = 0$
$\boldsymbol{\omega}$	$\omega = f(u_\tau, \dots)$	$\frac{\partial \omega}{\partial \xi_B} = 0$	$\omega = Constant$	$\frac{\partial \omega}{\partial \xi_B} = 0$

When using CFD both modelling and numerical errors are introduced. To ensure that the gained results are agreeing with physical reality, firstly the numerical errors must be determined. This is made by a verification technique, which will be further described in Systematic Grid Variations on page 11. Verification means checking that the gained solution agrees with the continuous mathematic model. Having made sure that the numerical errors are within a reasonable range, a validation should be made against experimental data, in this case wind tunnel measurements.

3.1.1 Meshing

The automatic meshing tool in SHIPFLOW could not handle the meshing of the geometries of keel 3 and 4, instead manual meshing in the software ICEM from ANSYS was used. For enabling a correct comparison between all keels, this technique was used for all meshing.

Throughout the meshing of the keels, emphasis was put on making the meshes structured and as similar as possible. Close to the keels the mesh was made dense in normal direction to catch all flow features within the boundary layer. The distance to the first cell wall was set to a value less than 0.0054mm which corresponds to a y^+ value of 0.6. This was in order to be able to perform grid coarsening for a grid dependence study, and still be below y^+=1 to correctly get all flow features from the boundary layer. The grid lines were also made orthogonal to the keel surface in this area everywhere that it could be achieved.

In order to make the CFD case directly comparable to the wind tunnel results a model of the wind tunnel was used as outer domain for the meshes. The exact cross-section was used but the length was extended in order to make the flow in the calculations to become fully developed from the inflow before reaching the keel.

Multiblock meshing was used in order to keep the structure of the meshes. In areas of interest such as the trailing edge, all sharp corners and areas of high curvature the meshes were made denser to ensure that all interesting flow effects were captured. The idea from the beginning was to mesh the keel together with the wind tunnel, but after some discussion with our supervisor Michał Orych it was decided to mesh the wind tunnel separately and then use a meshed body around each keel. This introduced an overlapping grids system, but it gave the advantage of making multiple runs with different angle of attack for the same meshes. The overlapping grids were solved by XCHAP.

Boundary conditions were defined in SHIPFLOW. For the keels, NOSLIP condition was used. For all outer boundaries, except for the in- and outflow, SLIP condition was used. All other boundaries were non-defined and therefore calculated as INTERIOR.

For the finest grids for the keels approximately 3 million cells was used. The wind tunnel was allowed to have a less dense mesh and was in total 0.5 million cells. These mesh sizes were chosen when it was assumed to give a sufficient precision without giving unreasonably high computational time.

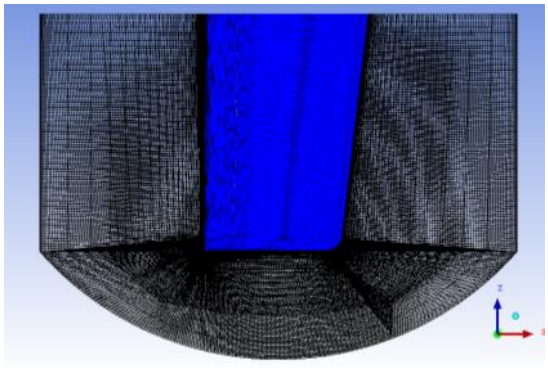

Figure 10: Mesh Keel 1

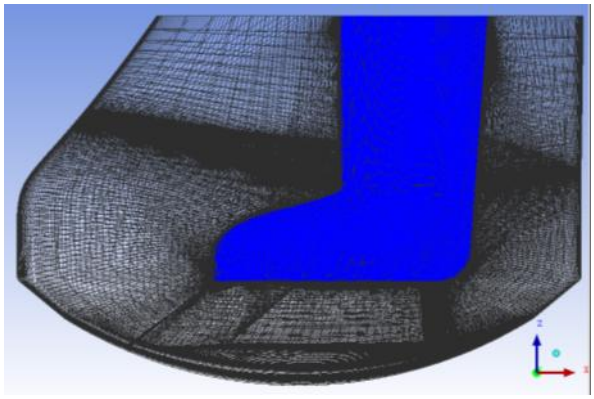

Figure 11: Mesh Keel 2

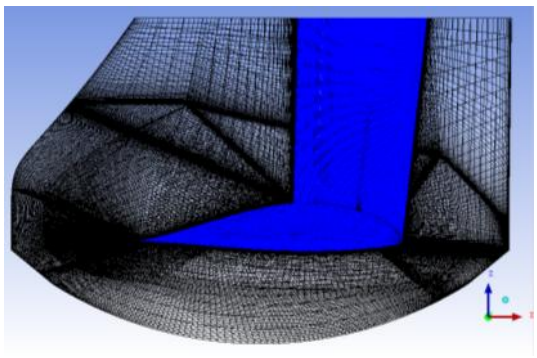

Figure 12: Mesh Keel 3

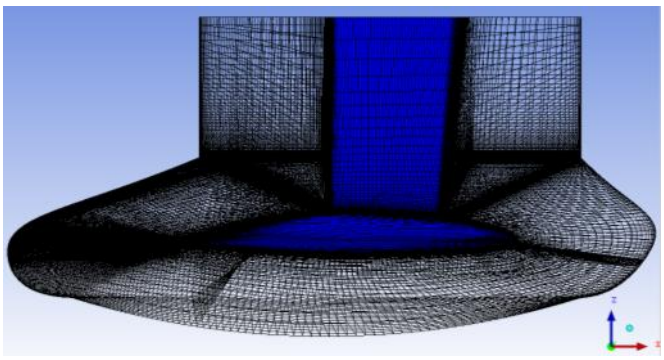

Figure 13: Mesh Keel 4

Figure 10 to Figure 13 shows the mesh for each keel together with the body. Only half of the model was meshed in ICEM. It was then mirrored in SHIPFLOW and merged with the wind tunnel. The same wind tunnel was used for all the keels. Perspective views of the meshes are shown in appendix C.

3.1.2 Calculations

For the CFD calculations the finite volume RANS solver XCHAP in SHIPFLOW was used [7]; [8]. The program uses ROE flux discretization, and the discretized equations are solved by an ADI-solver (Alternating Directions implicit) with the initial guess from the boundary conditions.

XCHAP uses an Explicit Algebraic Stress Model, EASM, as standard turbulence model. This model contains non-linear terms in order to model the viscous eddies, and it is one of the most accurate and advanced turbulence model available.

Parameters solved by XCHAP are, as found in the manual [7]:

- Velocity field
- Pressure
- Turbulent kinetic energy and specific turbulent kinetic energy
- Local skin friction coefficients
- Friction and pressure resistance coefficients for the keels

The blocks in the multiblock meshes were butt-joined, and block joints were avoided in areas of predicted high pressure and velocity gradients when the information travels with a slightly different speed across these compared to within the blocks.

For further information about the software we refer to the User manual of SHIPFLOW [8] and XCHAP [7].

3.1.3 Systematic grid variations

In order to ensure that the results are reliable some verification of the solutions was needed. There are several different methods that give solution verification. The two methods which were used in this master's thesis, the Factors of Safety (FS) method and the Least Squares Root (LSR) method, are described below. Both methods have been used in order to gain a higher accuracy of the verification. All theory in this section is based on two papers, reference [9] and [10].

Since the meshes for the different keels were similarly designed, a grid dependence study was only made for keel 4 which was considered to be most difficult to mesh. If this would pass the requirements the other meshes were considered to also be fine enough.

FS method

For this method, three systematic similar grids are needed. The iterative uncertainty U_1 should be at least one order-of-magnitude smaller than the grid spacing uncertainty U_G. In the convergence study, the refinement ratio, r, is defined as:

$$r = \frac{h_2}{h_1} = \frac{h_3}{h_2} \tag{1}$$

Whereh_1, h_2 and $h_3$are the grid spacing for the fine, medium and coarse grids. If the solutions for the grids are S_1, S_2 and S_3, the solution change, ε, for the medium-fine and coarse-medium and the convergence ratio R are defined as:

$$\varepsilon_{21} = S_2 - S_1, \quad \varepsilon_{32} = S_3 - S_2, \quad R = \frac{\varepsilon_{21}}{\varepsilon_{32}} \tag{2}$$

The Richardson Extrapolation (RE) method is used to estimate the order of accuracy p_{RE} and the error δ_{RE}. RE is only used when monotonic convergence, $0 < R < 1$, is achieved and then it is used to express the numerical solution with a form of power series.

$$S_i = S_0 + \alpha h_i^{p_{RE}} \tag{3}$$

Where S_i is the solution to the i:th grid, S_0 is the extrapolated solution to the zero step size, α is a constant and p_{RE} is the order of accuracy. In the numerical solution p_{RE} and δ_{RE} can be expressed as:

$$p_{RE} = \frac{ln(\varepsilon_{32}/\varepsilon_{21})}{ln(r)}, \quad \delta_{RE} = S_i - S_0 = \frac{\varepsilon_{21}}{r^{p_{RE}} - 1} \tag{4}$$

The general form of the uncertainty proposed by Roache [11] is: $U_{FS} = FS|\delta_{FS}|$ where FS is a safety factor. The FS method adopts this but considers three factors of safety according to the P value,$P = P_{RE}/P_{th}$: $FS_0(P = 0)$, $FS_1(P = 1)$ and $FS_2(P = 2)$. The estimated uncertainty with the FS method:

$$U_{FS} = FS(P)|\delta_{RE}| = \begin{cases} [FS_1 \cdot P + FS_0 \times (1 - P)]|\delta_{RE}|, & 0 < P \leq 1 \\ [FS_1 \cdot P + FS_2 \times (P - 1)]|\delta_{RE}|, & P > 1 \end{cases} \tag{5}$$

The recommended values for FS_i according to Tao and Stern [9] are: $FS_0 = 2.45$, $FS_1 = 1.6$ and $FS_2 = 14.8$. With these values the final FS method will have the follow appearance:

$$U_{FS} = FS(P)|\delta_{RE}| = \begin{cases} (2.45 - 0.85P)|\delta_{RE}|, & 0 < P \leq 1 \\ (16.4P - 14.8)|\delta_{RE}|, & P > 1 \end{cases} \tag{6}$$

LSR method

This method is also based on the Richardson Extrapolation (RE).It is claimed that the iterative error should be at least two orders of magnitude smaller than the discretization error. The Least Squares Root approach is used to determine the error and the order of accuracy. Estimation of the discretization error, ε, using RE is given by:

$$\varepsilon \approx \delta_{RE} = S_i - S_0 = \alpha h_i^{p_{RE}} \tag{7}$$

S_i = any integral of local quantity, S_0 = the estimation of exact solution, h = typical cell size in the grid, α = a constant and p_{RE} = the observed order of accuracy. To be able to estimate the error, ε, the unknown parameters; S_0, α and p_{RE} has to be solved using the data from at least four different grids. The theoretical order of accuracy is supposed to be p_{RE}=2, but usually it differs a bit. The uncertainty, $U_\emptyset$, is depending of the value of p_{RE}.

-Monotonic convergence

$$\begin{aligned} &0.95 \leq p_{RE} \leq 2.05: && U_\emptyset = 1.25\delta_{RE} + U_s \\ &p_{RE} \leq 0.95: && U_\emptyset = min(1.25\delta_{RE} + U_s, 3\delta_{RE}^{12} + U_s^{12}) \\ &p_{RE} \geq 2.05: && U_\emptyset = max(1.25\delta_{RE} + U_s, 3\delta_{RE}^{02} + U_s^{02}) \end{aligned} \tag{8}$$

The values used to calculate the uncertainty can be found by using the following equations:

$$\delta_{RE}^{02} = S_i - S_0 = \alpha_{01} h^2 \tag{9}$$

$$\delta_{RE}^{12} = S_i - S_0 = \alpha_{11}h + \alpha_{12}h^2 \quad (10)$$

$$\frac{h_i}{h_1} = \sqrt{\frac{(N_{cells})_1}{(N_{cells})_i}} \quad (11)$$

There are two other convergence conditions:

-Oscillatory convergence: (12)

$$U_{\emptyset} = 3\delta_{\Delta M}$$

-Anomalous behaviour: $$U_{\emptyset} = min(3\delta_{\Delta M}\,, \quad 3\delta_{RE}^{12} + U_s^{12}) \quad (13)$$

$$\delta_{\Delta M} = \frac{\Delta_M}{\left(h_{n_g}/h_1\right)-1},$$

where $\Delta_M = max\left(|S_i - S_j|\right) \quad 1 \geq i,j \geq n_g$

The values of U_s, U_s^{02} and U_s^{12} are standard deviations of curve fit for equation (7), (9) and (10)

Results from systematic grid variation

Three new grids for keel 4 where created in ANSYS ICEM. The constant $\sqrt[4]{2}$ where used to scale the original grid. In Table 2 the different grids are presented with number of cells and number of points.

Table 2: Number of cells and points for the four different grids in the uncertainty analysis

Grid	Number of cells	Number of points
Original	3904668	3380982
Grid 1	2453258	2020370
Grid 2	1481872	1199812
Grid 3	931128	726552

Only three grids are used in the FS method and they fulfilled the criteria that the iterative uncertainty should be at least one order-of-magnitude smaller than the grid spacing uncertainty. Unfortunately no monotonic convergence was achieved so the RE method could not be used.

For the LSR method all four grids were used. The iterative error has to be two orders of magnitude smaller than the discretization error. This was not achieved. Similarly as for the three grids no monotonic convergence was gained.

The conclusion from this is that the uncertainty analysis did not work. It is very important that the grids are geometric similar and this is probably the reason to that the uncertainty analysis did not work. When manually creating the grids in ANSYS ICEM it is very hard to get the exact same geometric appearance on all the grids.

3.1.4 Results

In this results part conclusions from the CFD post processing are presented. Images displaying pressure distribution and the velocity field around the keels have been extracted from TECPLOT, and are commented here. A discussion concludes the different aspects and performance after the result part. A presentation of the force results and a comparison of the CFD and wind tunnel measurements are found in the global results part on page 35. For all figures where the legend says "velocity", note that this is the total velocity vector: velocity=$\sqrt{V_x^2 + V_y^2 + V_z^2}$

Keel 1, 0° angle of attack

Since there is no bulb attached but only a fin the velocity field is very even in vertical direction and the boundary layer builds up very similarly along the whole fin. Around the tip region a tip vortex is created which can be seen in the velocity field behind the keel. The pressure distribution is even and the low pressure regions in Figure 14 can easily be compared to the high velocity regions in Figure 15.

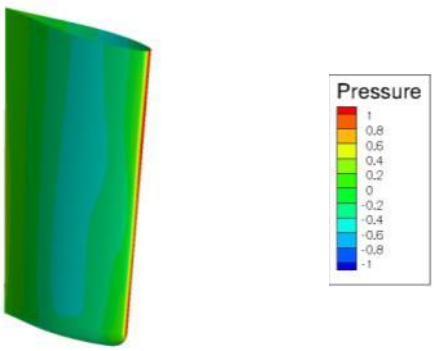

Figure 14: Keel 1 Pressure distribution

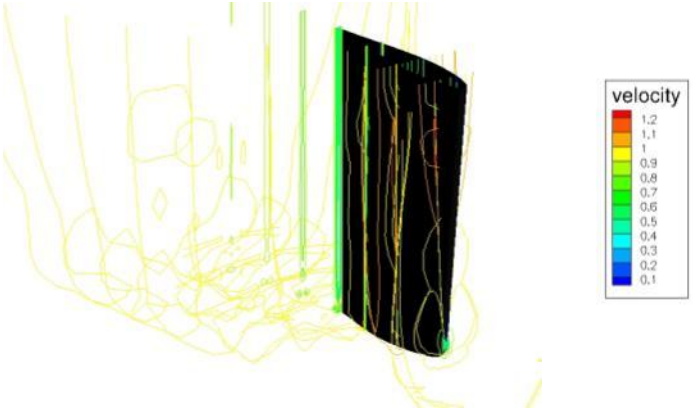

Figure 15: Keel 1 Velocity field

Keel 2, 0° angle of attack

These results could not be gained using our mesh due to a problem in the solver which only occurred for 0˚ angle of attack. Results were therefore gained from Kasper Ljungqvist [12] who in his Master's Thesis used the automatic meshing tool in the SHIPFLOW software. The gradual thickening of the keel profile of keel 2 allows the pressure to smoothly and gradually change over the keel and bulb surface as seen in Figure 16. The boundary layer develops evenly, as seen in Figure 17, and creates a long tip vortex in vertical direction due to the vertical cut off of the trailing edge of the keel.

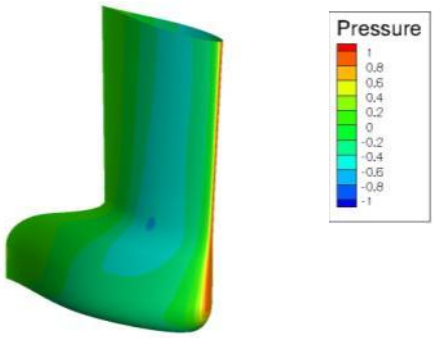

Figure 16: Keel 2 Pressure distribution

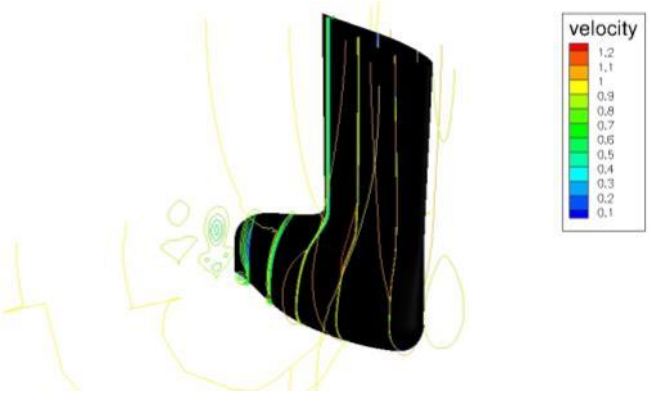

Figure 17: Keel 2 Velocity field

Keel 3, 0° angle of attack

Keel 3 has a quite deep pressure drop at fin mid chord where the fin connects to the bulb, and the forward stagnation point from Figure 18 can be found affecting the velocity field in Figure 19. This is the starting point for the increase in velocity which creates a vortex high up behind in the wake. For this zero angle of attack case the flow stays attached to the bulb all the way back to the beaver tail, and does not create any major vortex in the wake from there.

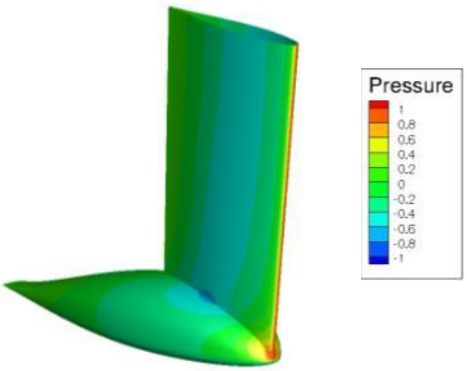

Figure 18: Keel 3 Pressure distribution

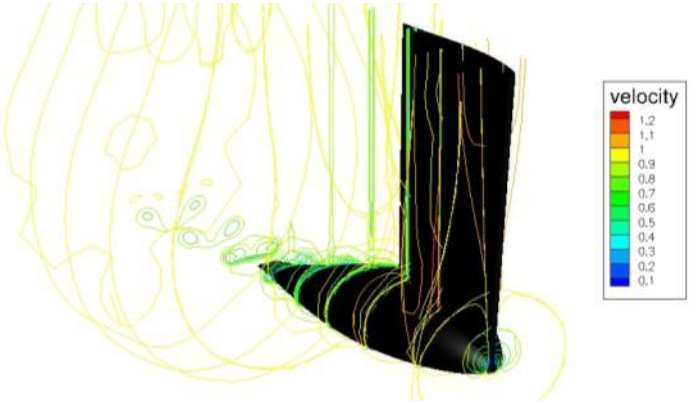

Figure 19: Keel 3 Velocity field

Keel 4, 0° angle of attack

Keel 4 has also an evenly distributed pressure and builds up a boundary layer which stays attached until the trailing edge of both the fin and the bulb. One can spot the difference between this and keel 3 since the flow reattaches from the fin end to the bulb, and no vortex can be found there. However when the flow separates behind the beaver tail, a double tip vortex cab be found, but is disappears not far behind in the wake. On the velocity field in Figure 21 it can be seen that something has upset the solver at mid span of the fin, there is an inconsistency in the velocity field which would mean there is a pressure drop which should not be found there. This should not affect the total drag extensively, and since no extraordinary flow features are expected here, it will not be further analysed.

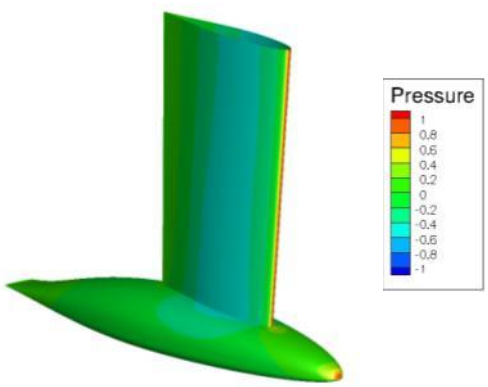

Figure 20: Keel 4 Pressure distribution

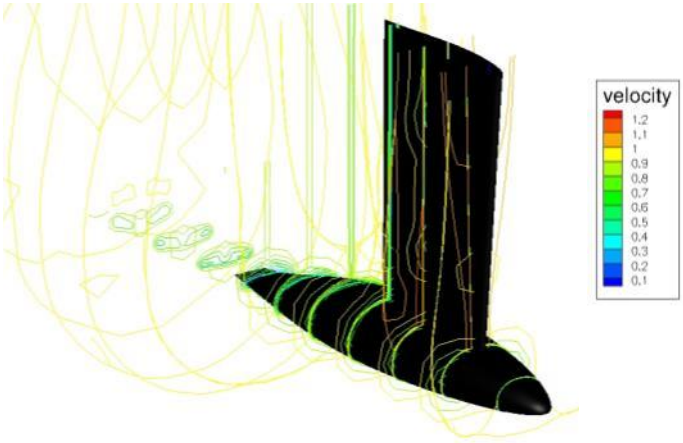

Figure 21: Keel 4 Velocity field

Keel 1, 4° angle of attack

As seen in Figure 22, and as expected, keel 1 has an evenly distributed pressure distribution also for four degrees angle of attack. From the velocity distribution in Figure 23 the boundary layer builds up and creates a small tip vortex behind the keel. There will always be a cross-flow around the tip of a keel, but due to the properly designed hard chine along the tip of the keel, this tip vortex may have been reduced somewhat compared to that of a rounded tip. The vortex is also kept at a low position due to the chine.

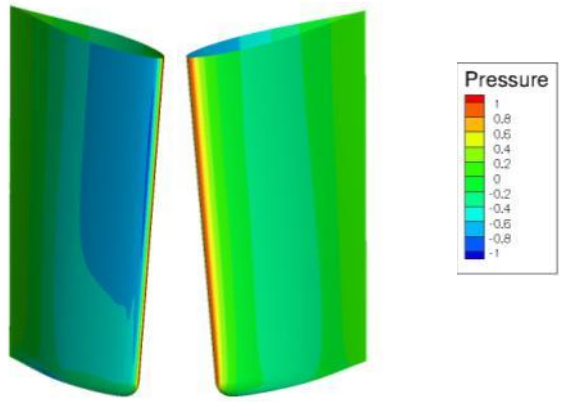

Figure 22: Keel 1 Pressure distribution. Left: Suction side; Right: Pressure side

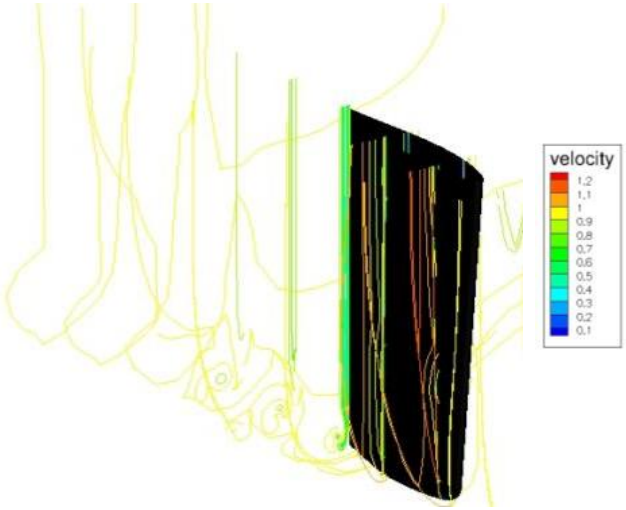

Figure 23: Keel 1 Velocity field

Keel 2, 4° angle of attack

As seen in Figure 24 the pressure distribution is smooth along the side on keel 2. Because of the gradual thickening of the profile the isobars runs continuously down on the bulb part. In Figure 25 it can be found that this also results in a down flow which creates relatively large tip vortex behind the keel extending in vertical direction. On the leading edge the most significant stagnation point occurs just above the bulb part, but the velocity field evens out further aft on the bulb. The difference between a beaver-tail and this long vertical cut off can clearly be seen. The boundary layer is relatively thin on

the lower part of the fin when the flow is pushed down and stays attached to the bulb. Worth noticing is how the integrated design will gain higher lift due to that the bulb part contributes to the lift by the larger pressure difference between the sides.

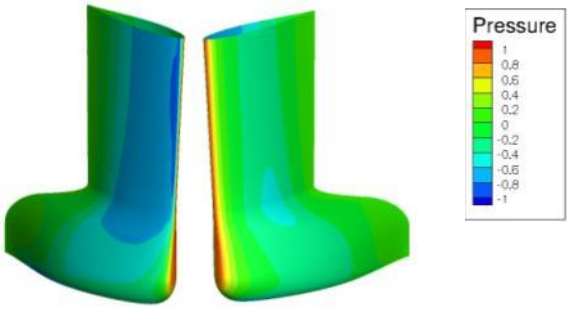

Figure 24: Keel 2 Pressure distribution. Left: Suction side; Right: Pressure side

Figure 25: Keel 2 Velocity field

Keel 3, 4° angle of attack

In Figure 26 it can be seen that keel 3 has a large stagnation zone where the fin and bulb meet the flow. Here it can be seen that the bulb influences the pressure on the suction side which decreases the pressure difference and hence the lift. When the boundary layer separates from the bulb a double tip vortex occurs. This behaviour can be explained by the beaver tail which keeps the flow attached to the aft part of the bulb. However the double tip vortex turns into a larger, single tip vortex which can be seen at the aftermost velocity contour in Figure 27.

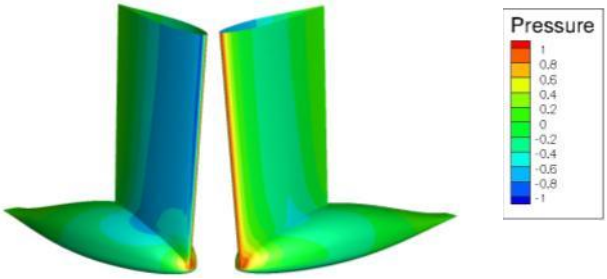

Figure 26: Keel 3 Pressure distribution. Left: Suction side; Right: Pressure side

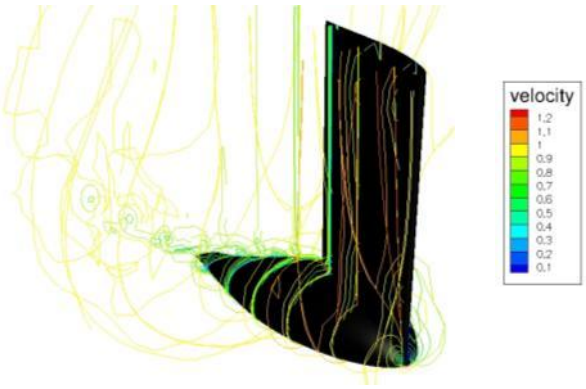

Figure 27: Keel 3 Velocity field

Keel 4, 4° angle of attack

In Figure 28 the evenly distributed pressure can be followed. On this design the bulb does not affect the pressure difference and hence the lift is not decreased. For this keel, a separate stagnation point occurs for the bulb and the fin. From the stagnation point on the bulb, the flow follows smoothly and a gradual boundary layer is built up. As hoped for in the designing of the keel, the flow along the fin and the bulb are relatively unaffected by each other until after the trailing edge of the fin. Seen in Figure 29 the large separation in the old design (compare with Figure 31) is now absent, and first at the aft tip on the bulb a similar double tip vortex as seen on keel 3 occurs.

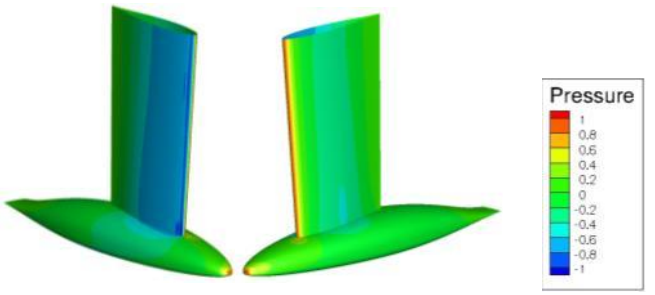

Figure 28: Keel 4 Pressure distribution. Left: Suction side; Right: Pressure side

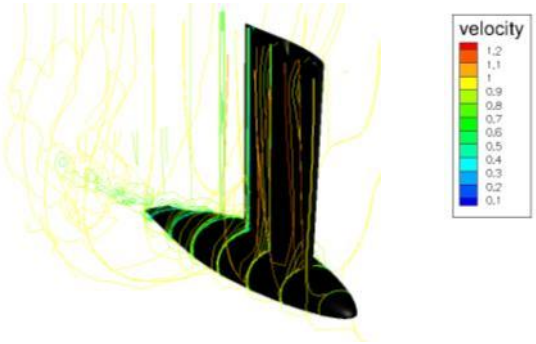

Figure 29: Keel 4 Velocity field

Old design of Keel 4, 4˚ angle of attack

As mentioned in the introduction, the poor behaviour of the old keel 4 was suspected to origin from a large separation on the suction side. In Figure 31 this separation can clearly be seen.

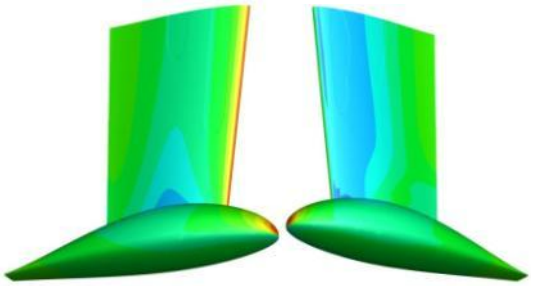

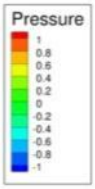

Figure 30: Old keel 4 Pressure distribution. Left: Suction side; Right: Pressure side

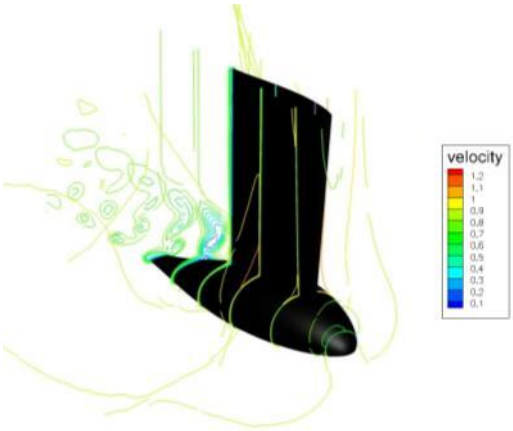

Figure 31 Old keel 4 Velocity field

3.1.5 Discussion

For all cases similar meshing was tried to be achieved. For all solutions except for keel 2 in 0˚ of attack the convergence was satisfactory, and the results gained were found to be reasonable. All data were analysed using TECPLOT and presented in a simple but understandable way. A presentation of several slices individually from all cases was not made due to space issues. A comparison between the results gained from CFD in numbers with the results gained from the wind tunnel tests can be found in the global results and discussion on page 40 and 42.

3.2 Wind Tunnel Testing

To validate forces gained from CFD calculations, tests were performed in the wind tunnel of Applied Mechanics at Chalmers University of Technology. The aim and purpose of the tests was to measure the forces acting on the keels (Lift and Drag forces).
The operating speed for the wind tunnel was set to 40m/s. This gave an R_n of approximately $1.4 \cdot 10^6$ for the model tests using the mean chord length for keel 1. This equals 1/3.5 of full the scale keels.

The wind tunnel has a measuring section of [B H L] = [1.8 1.25 2.7] with a free stream turbulence intensity of 0.1% at full speed. The cross section increases slightly downstream to compensate for the boundary layer build up along the walls. A photo of the wind tunnel cross-section can be seen below in Figure 32.

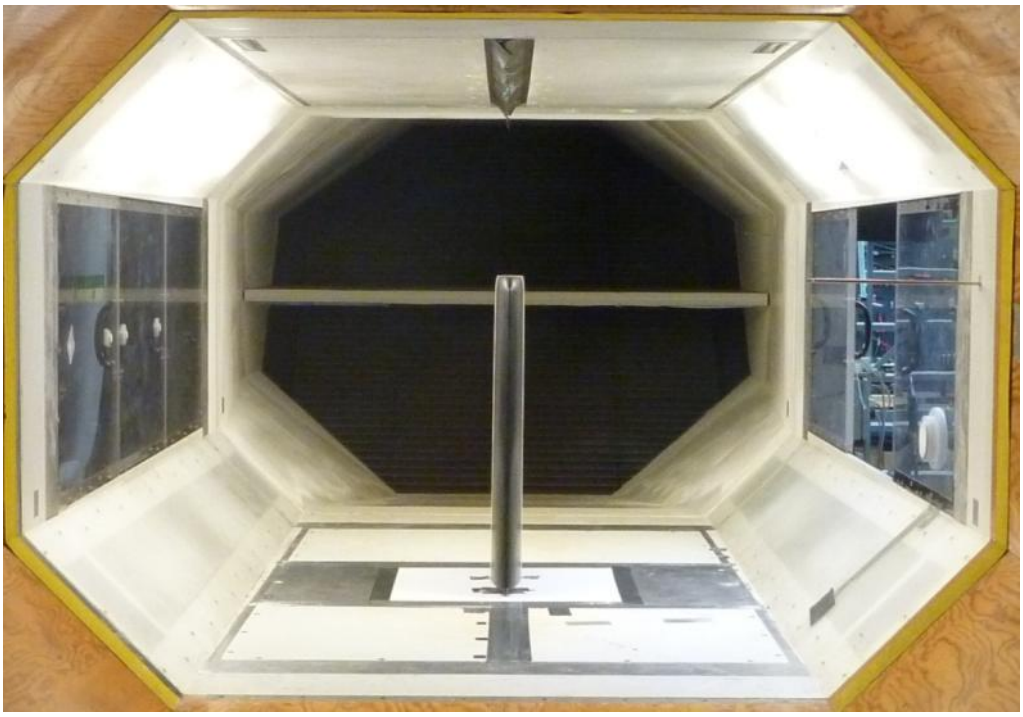

Figure 32: Wind tunnel cross-section; photo taken from upstream with keel 1 in measuring position

3.2.1 Method

For the measuring of the forces a 6-component strain-gage balance from RUAG [13] was used. As the aim of the wind tunnel testing was to validate the forces on the keel no measurements were made of pressure or velocity close to the keel models.

The complete representative flow of data from the wind tunnel testing can be seen in Figure 33 below.

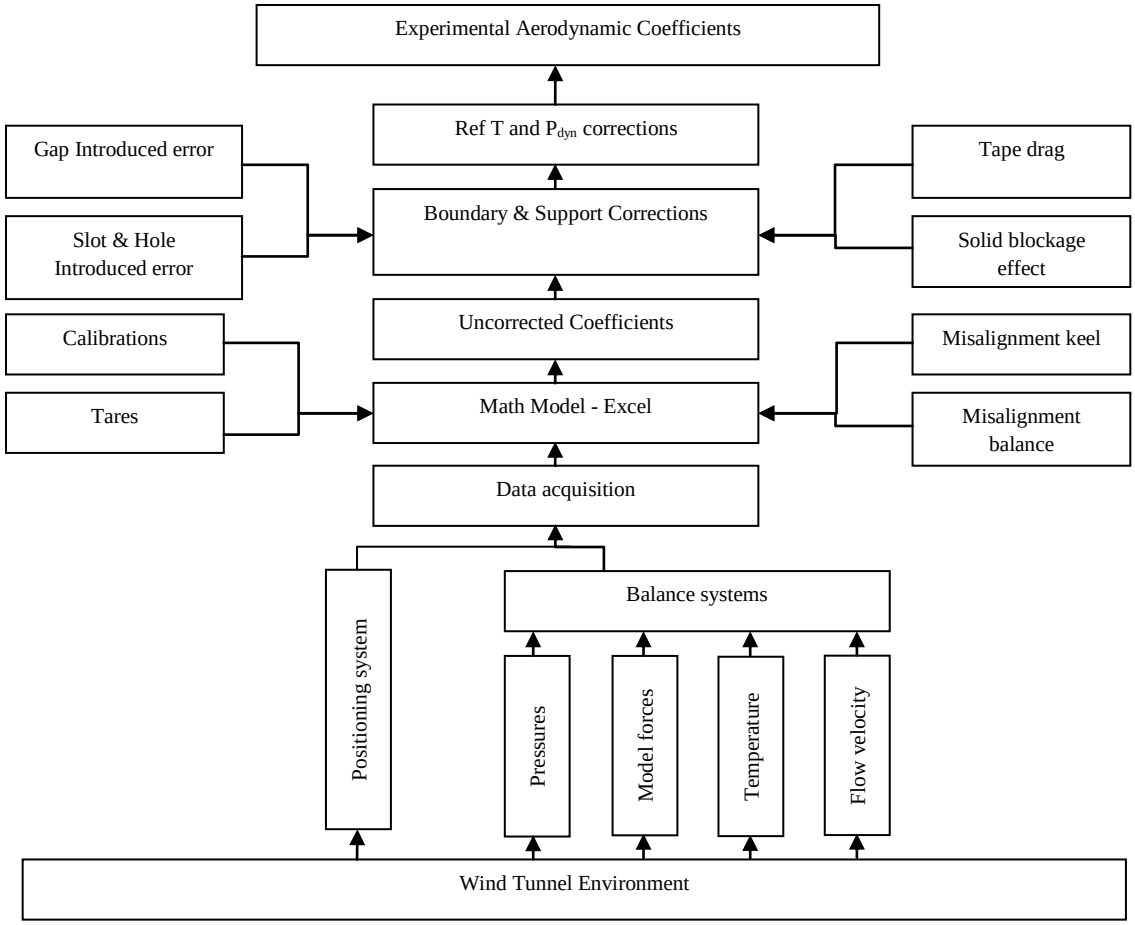

Figure 33: Representative data flow for Wind Tunnel tests [14], modified for this master's thesis.

3.2.2 The Models

The final keel models were manufactured in scale 1:2.5 in a CNC-machine with high precision. The material used was Necuron 651 with a density of 700kg/m^3. The surface was sanded. A rod was inserted in each keel at 25% of the base chord length by the manufacturer for the mounting of the keels on to the balance. The tolerance for the position of the rod was 0.01mm in y-direction which was considered to be very good. In Figure 34 to Figure 37 the keel models can be seen. The white strip is a tape for tripping the flow forcing transition, and it is described in the following section.

Figure 34: Keel 1

Figure 35: Keel 2

Figure 36: Keel 3

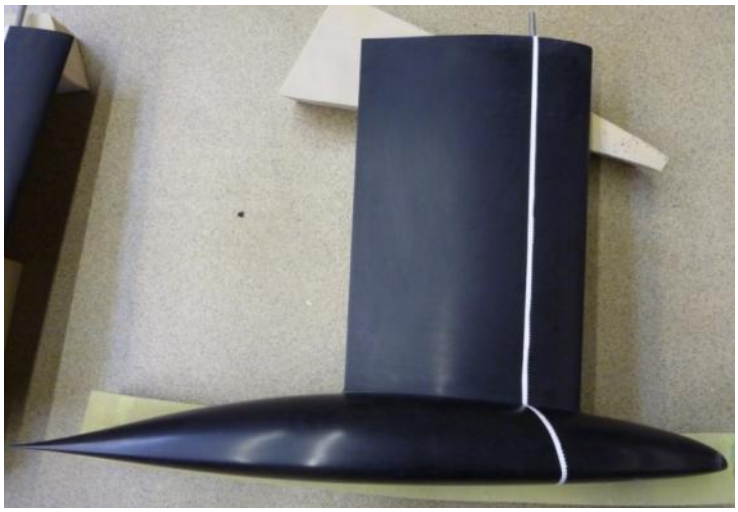

Figure 37: Keel 4

3.2.3 Set-Up

The keel models were mounted on the balance with a rod stiffly connected between keel and balance. For avoiding a large moment inside the keels, an additional rod was put closer to the trailing edge. This rod was clamped between the keel and a plate which was bolted to the balance.

Both rods went through the wind tunnel floor and were carefully checked for moving free without touching the floor plate. The forward rod went through a hole in the floor since this was located in the centre of the turn table. The aft one went up through a slot for enabling a +/- 4° turn of the keel.

The balance was mounted onto a turning table to make measures for different angles of attack possible. The rotation angle was measured with an approximated precision of 1/7°.

Since the keels were relatively heavy weighting around 17kg, and the centre of gravity was located further aft than where the pre-mounted rod was put, the static moment on the balance was large. The dual support system minimized the moments inside the keels, but it still affected the balance. This moment was checked to be well within the range of the balance limits. Manual corrections from the

balance manufacturer's user guide [13] were also used to minimize induced errors from coupled moments and forces.

In Figure 38 a schematic model of the set-up can be seen, and in Figure 39 a picture of the set-up.

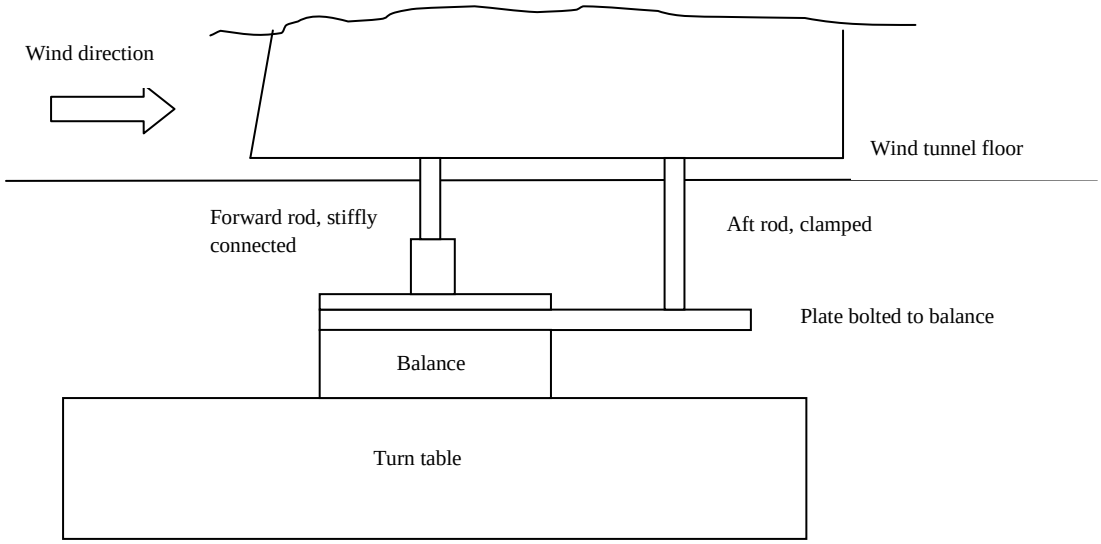

Figure 38: Set-up; side view

Figure 39: Set-up; Turn table with balance. The slot in the wind tunnel floor can be seen in the upper part of the picture. For the measurements the set-up was heightened and the aft rod was mounted.

R_n dependence

The difference in R_n between full scale and model scale implicates that a number of important viscous effects are not scaled properly. The main ones are friction drag, transition, trailing edge separation and laminar leading edge bubbles.

The CFD was run at model scale, so the effects of the frictional drag would not cause any problems. The CFD method used was as mentioned RANS, and this does not calculate the laminar boundary

layer. Hence, forcing of the transition was considered necessary, and this also solved the possible problem with leading edge bubbles as the tripping devices were put in front of the positions where the earliest bubbles were expected.

For forcing the transition a zigzag tape of 0.30 mm was used. This would according to investigations made in a Doctoral thesis by Sofia Werner [15] force the transition but affect the drag and keel profile minimally. A method recommended by Prof. Larsson was used to evaluate this method. The method included a stethoscope together with a pitot tube which was used to listen to the flow before and after the tape. There was a significant difference in the sound from before and after the tape which could only origin from the transition, and therefore the tape was confirmed as being able to force transition. The tape was put at around 25% chord length of the fin, and then stretching down over the bulb. The positions on the bulbs were between 10-25% differing slightly between the keels. The distances used for the different bulbs were considered to be in front of the position where the first bubbles were expected, and as long as this was fulfilled a continuous taping was seen as more important than an exact position for all keels. A picture of the zigzag tape can be seen in Figure 40.

The trailing edge separation was avoided by not taking any measurements when overloading the keels. Trial runs were made which gave the stall angle of the keels to around 20° angle of attack, which shows that measuring points at around 5° angle of attack were definitely in the safe region.

Figure 40: Zigzag tape

3.2.4 Testing

The keels were placed as closely aligned with the wind tunnel as visually possible. The forces for the assumed zero angle of attack were measured as well as for angles stepwise to +/- 5°. This interval was chosen to clearly see the trends of the forces, and to ensure to cover the +/- 4° values which would be used for the validation of CFD. Hence, one test series contained eleven measuring points. 15 samples were recorded for every point with a 5 seconds interval for averaging away momentary fluctuations. At least three complete test series were completed for each keel.

Finding keel zero angle of attack

The keel zero angle of attack was found by searching the minimum value of the total forces squared, using the forces X and Y from Figure 41. When the keel is aligned with the flow it will only have a drag force, the lift is zero, and the sum of the total forces squared is then minimal.

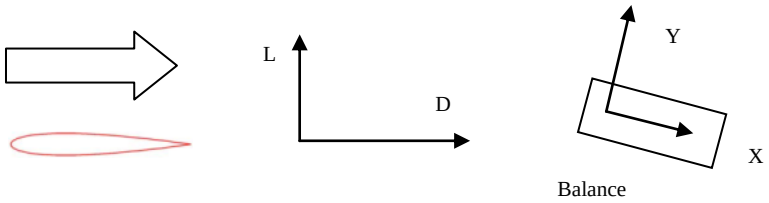

Figure 41: ***Keel in zero angle of attack, the position on the turn table was derived for later plotting of forces.***

The position measured on the positioning system on the turn table where m*in*(X^2+Y^2) occurs, or more easily interpreted where the line,

$$y = \sqrt{X^2 + Y^2} * \sqrt{|X|/X} \tag{14}$$

plotted against measured position crosses the X-axis, gives the position of zero angle of attack for the keel. This zero was later used for the plotting of L and D against angle of attack, it should however be noted that it was not used for deriving these forces from the measured forces X and Y.

With a different method it might have been possible to find the position of balance zero by using the keel zero angle. This by using the following formula:

$$L = -X \cdot \sin\beta + Y \cdot \cos\beta = 0 \rightarrow \beta = \tan^{-1}\left({}^{Y}/_{X}\right) \tag{15}$$

$$D = X \cdot \cos\beta + Y \cdot \sin\beta$$

The angle between balance and keel could easily had been found by taking $\beta = arc\ tan(Y/X)$ in position of keel zero. However since no measurements existed for this exact position, another method had to be used which is described below. This need for another method origin from the lift force having a higher gradient than the drag force in the region, and if interpolating the measured values, even a slight misalignment will give an unreasonably large calculated angle.

Derivation of L and D

When having a balance mounted on the rotating turn table, the forces measured X and Y will vary with the keel angle of attack. To get the forces L and D an angle transformation was introduced. The balance zero was assumed to be at a position which was found by measuring forces on a rod, and turning the set-up until only an X-force existed. This method was not considered perfectly accurate, and a misalignment angle was introduced to correct this zero position. This misalignment angle was corrected for according to Figure 43.

Note that whichever angle the keel had, the forces measured by the balance were always transformed to the wind tunnel coordinate system and the keel angle of attack was only then used for plotting these.

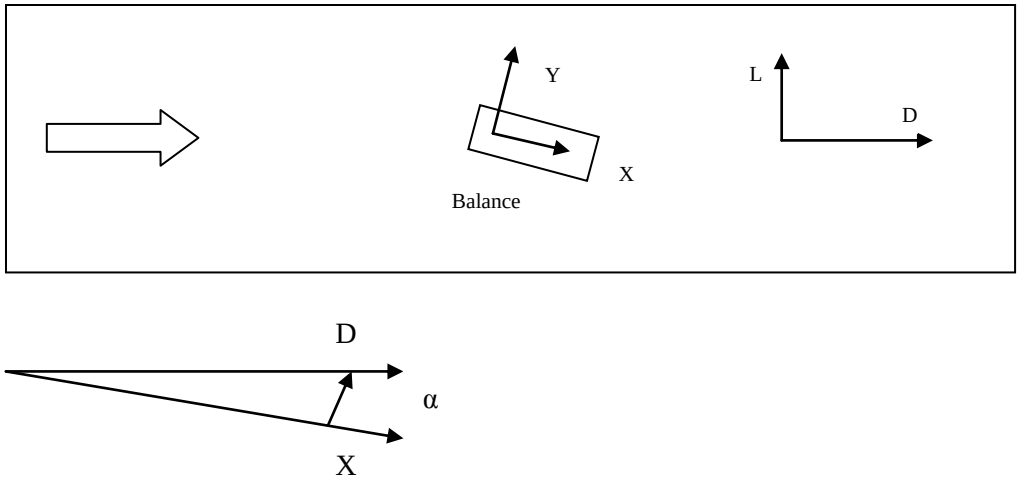

Figure 42: ***Coordinate systems of balance and wind tunnel with measured angle***

The forces L and D, by conversion of X and Y using the angle α from Figure 42:

$$D = X \cdot \cos(\alpha) + Y \cdot \sin(\alpha) \tag{16}$$

$$L = -X \cdot \sin(\alpha) + Y \cdot \cos(\alpha)$$

The angle α contains both of the wanted angle and a misalignment angle.

3.2.5 Analysis

After the measurement series was performed, the recorded data was analysed in Microsoft Excel to derive the corrected aerodynamic coefficients as described in Figure 33. After the proper corrections described in the following part had been made, the values were plotted into graphs. In order to get the trends of the measurement series a curve was then fitted to the values. Examples of measurement scatter, curve fittings and different corrections made are described in the following section.

Uncertainty analysis

As with all types of measurements, a measured value cannot be known to provide an absolute true result. In this analysis, a division into three groups of components that contributes to variation of the results have been chosen:

- Bias errors – systematic errors that can be analysed and to some extent corrected
- Precision errors – random errors which can be presented as mean value and standard deviation of the measurements, but not corrected for
- Errors which cannot be quantified, hence they are only described but not analysed further

Also there is a significant difference in comparing absolute values with trends. Comparing the measurement results between the four different keels exclude the bias even without correction when they are assumed to share the same bias errors. This is known to be a "common practice" from the ITTC guide [15] even if it is not exactly true. However, the comparison between the measurements from the wind tunnel with computed results from CFD required that the bias errors were corrected for.

Table 3 describes the bias errors, and the corrections made. If a bias error remained after making the correction, and if this remaining error was possible to quantify, it is listed in Table 4 which states the uncertainties for a single measurement.

Table 3: Bias errors and corrections made

Source	Correction
Misalignment angle balance	CD correction
Misalignment angle keel	Force min. correction
Dynamic pressure dev. From ref.	DP correction
Tape drag	Tape drag correction
Boundary effects	BE correction
Slot interfering	Not quantifiable
Gap interfering	Not quantifiable
Uneven wind tunnel floor	Not quantifiable

Table 4: Uncertainties for a single measurement. Reference temperature is 25°C; reference pressure is 100.9kPa

Error source	Type	Size	Uncertainty Lift [N]	Uncertainty Drag[N]
Balance precision	precision		8,75E-02	9,50E-02
Balance zero calibration	precision		1,00E-02	1,00E-02
Angle measurement precision	precision	1/7°	2,50E-01	2,00E-02
Temperature	calibration	0,3°C	3,50E-03	7,00E-04
Static pressure	calibration	100Pa	1,50E-03	1,50E-03
Temp dev. from ref.	variation	4°C	4,40E-02	8,40E-03
Static pressure dev. from ref.	variation	900Pa	1,30E-02	1,30E-02
Misalignment angle, balance	precision	2/70°	2,20E-03	1,99E-02
Misalignment angle, keel	precision	1/70°	1,10E-03	9,90E-03
		Total	2,69E-01	1,01E-01

The precision errors are estimated to two times the standard deviation. The total uncertainty was calculated using the following formula:

$$U^2 = \sum_{j=1}^{N} b_j^2 \tag{17}$$

where b_j are the remaining bias uncertainties.

In the following sections the different bias errors are described in more detail, as well as the corrections made.

Definition of balance misalignment

To find the balance misalignment the derived force D was plotted against keel angle of attack. The keels are perfectly symmetrical, and therefore the value of D should be the same for +/- 4° angle of attack. By varying the misalignment angle in the excel file, this could be achieved. It was showed that the pre-tested zero differed from the corrected one with as much as 0.3°.

After correcting for this a precision of approximately 0.03° was gained. An example on this correction can be seen in Figure 43.

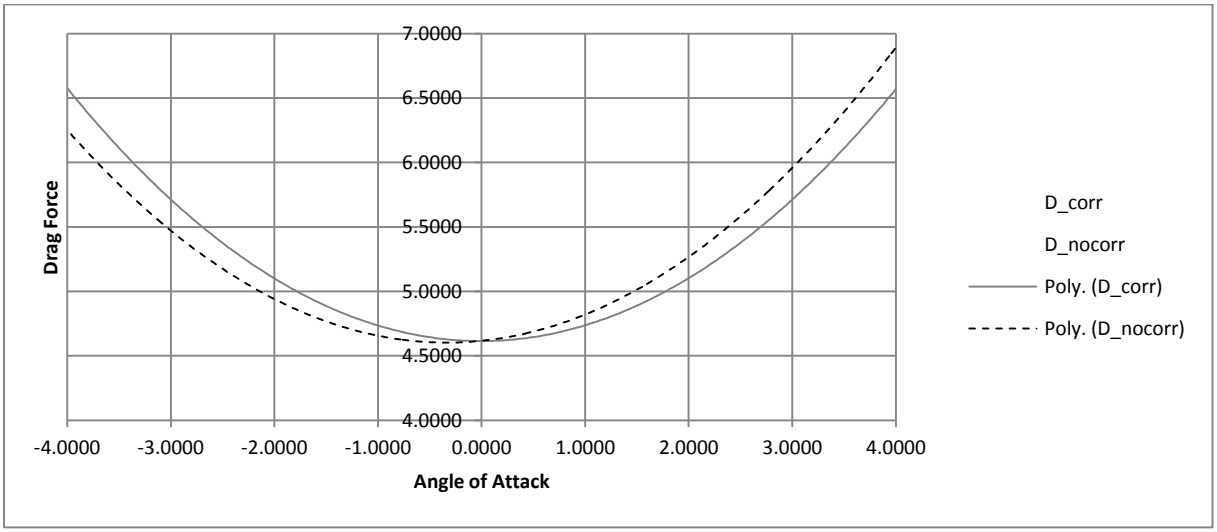

Figure 43: Drag curve correction: For this case a misalignment angle of 0.23° was corrected for.

Keel misalignment

After correcting the keel zero angle of attack according to equation (14) a precision of approximately 0.015° was gained, this remaining uncertainty originates from the curve fitting in Excel.

Gap between keel and wind tunnel floor

The gap between the keel and the wind tunnel floor has according Barlow et al. [14] to be below 0,005 times the span to have a negligible influence on the total drag. In the experiments of this master's thesis a gap of 4mm was used, which equals 0.0053 times the span. The reason for this comparatively large gap was to visually be able to ensure the keel never came in contact with the wind tunnel floor. Note that the floor plate tended to flex around 1mm when running the wind tunnel at 40m/s. An evaluation of forces versus gap size was made and the results can be seen in Figure 44 below. The difference between 4 and 5mm was found to be very small, hence the results were considered to be unaffected by this gap. The gap might still have had a slight influence on the forces, but there was no way of quantifying this.

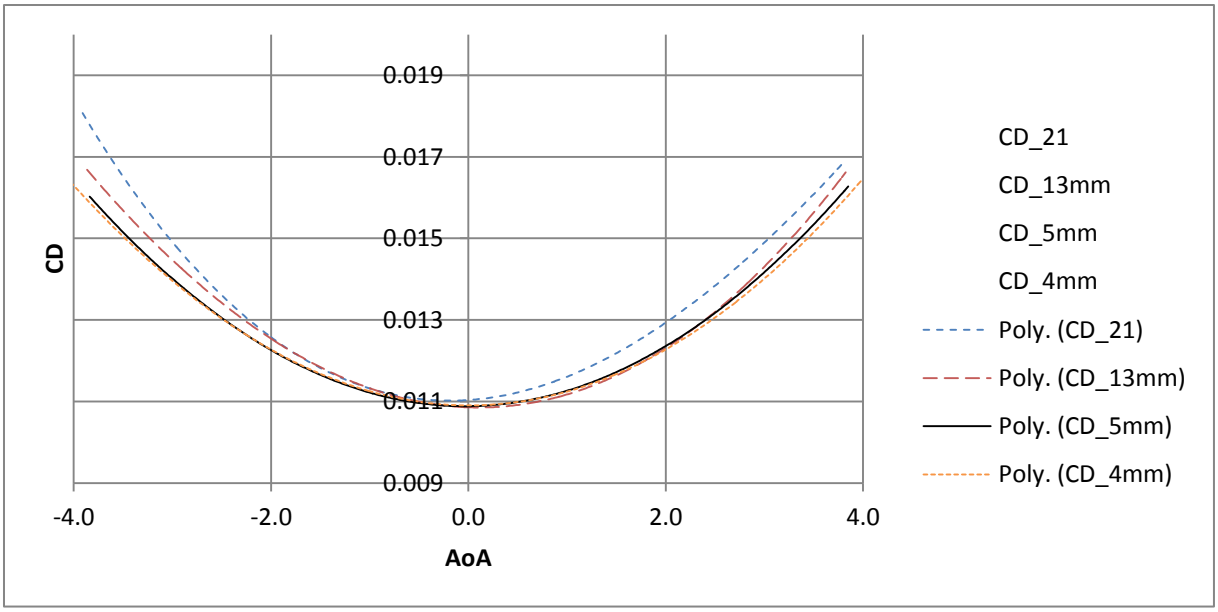

Figure 44: Comparative measurements with varied Gap-size

Slot and hole for connections

According to Ranzenbach et al. [16], the leakage of air through the slot might have a large impact on the results. The hole and slot which were kept at a minimal size while ensuring the rods never touched the wind tunnel floor.

A study of three measurement series with and without hole and slot taped over was made and it was found that the hole and slot did not affect the result significantly. The results for a complete test series with hole and slot taped over can be seen in Figure 45. For convenience the hole and slot were kept open to speed up the testing procedure. As with the gap, this might still have had a slight influence on the forces, but it was not possible to quantify this.

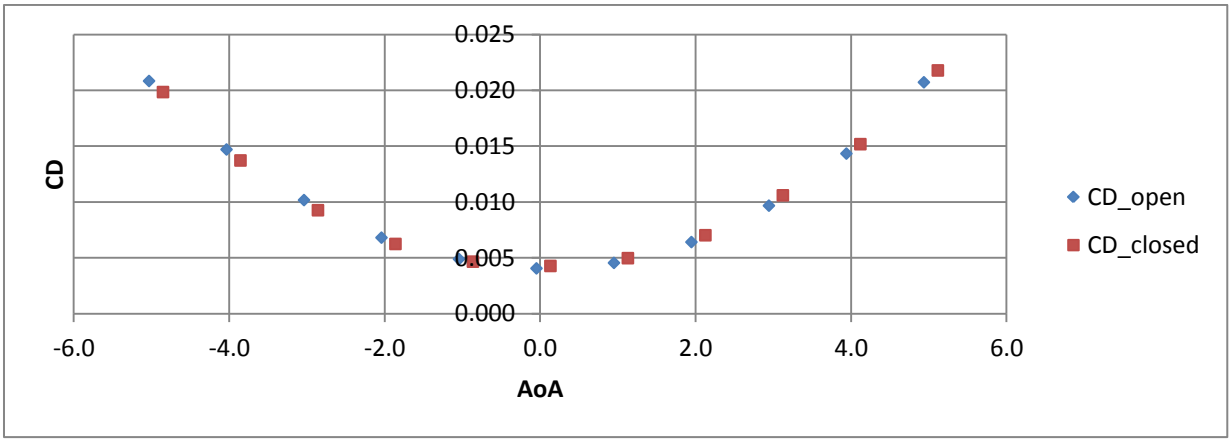

Figure 45: Comparison between measurement series with and without slots and hole

Dynamic pressure variation

The inlet velocity was kept virtually constant, but the density varied due to the static pressure and temperature varying with the conditions in the room. As L and D are R_n dependent, the forces were corrected using a reference dynamic pressure at 1200Pa for making an equal comparison possible.

$$F_{corr}=P_{dyn,ref}/P_{dyn}\cdot F \qquad (18)$$

Tape drag

The tape used for tripping the flow contributed to the total drag of the keels. As we used the tape thickness and method from Sofia Werner's Doctoral Thesis [15], and when our keels were in the same order of sizing as the model used in her thesis, a drag correction of 0.07N was subtracted from the total drag. This drag was calculated in the Doctoral Thesis using RANS simulations of fin and bulb with and without tape. In both cases the flow was laminar upstream of the tape, and turbulent downstream.

Boundary effects

There are four main boundary effects that according to Barlow et al. [14] have an effect on the results:

- Buoyancy effects
- Wake blockage
- Solid blockage
- Streamline curvature/downwash

The buoyancy effect can be neglected since the wind tunnels cross-section increases throughout the testing section, and this accounts for the boundary layer growth. Hence no longitudinal pressure gradient exists. Since only measurements were done for small angles of attack and the keels were scaled down to fit properly inside the wind tunnel, the flow can be assumed to be streamlined. Using Maskell's method [17] the correction for wake blockage of streamlined flow looks as follows:

$$\frac{\Delta V_{wb}}{V_U} = \varepsilon_{wb} = \frac{S}{4A_{WT}} C D_0 \tag{19}$$

Where A_{WT} is the cross sectional area of the wind tunnel, 2.043m^2, and S is the reference area of the wing on which CD_0 is based, which differs between the keels.

For our set up this value is largest for keel 1 at 4° angle of attack, and then equals around 0.001 which is negligible for our analysis.

The solid blockage can be derived from Thom's short form equation method [14]:

$$\frac{\Delta V_{sb}}{V_U} = \varepsilon_{sb} = \frac{k * KeelVolume}{A_{WT}^{3/2}} \tag{20}$$

where k=0.9 for a three dimensional wing. These values were larger than the wake blockage effect and were taken into account in the analyses. The exact values can be seen in Table 5.

Table 5: Solid blockage coefficients

	Keel Model Volume (m^3)	ε_{sb}
K1	0,044	0,0054
K2	0,062	0,0076
K3	0,061	0,0075
K4	0,060	0,0074

The fourth boundary effect is downwash. According to [16] the effect is negligible for models with spans up to 80% of the wind tunnel width, and therefore this effect was not included in the analysis.

3.2.6 Results

The results from the wind tunnel presented as comparison between the keels, and also with theoretically calculated values. C_D and C_L were non-dimensionalised with the lateral area, A_L of keel 1. The theoretical C_D and C_L are calculated using Prandtl's and Whicker and Fehlner's methods taken from [1] and [18]. They are using the aspect ratio AR, wetted surface S_w and A_L for keel 1 as follows:

$$C_{L,Prandtl} = \frac{C_{L,2D}}{1 + \frac{2}{AR}} \cdot \alpha \tag{21}$$

$$C_{L,WF} = \frac{C_{L,2D} \cdot \mathrm{AR}}{\left(2 + \sqrt{AR^2 + 4}\right)} \tag{22}$$

$$C_{DI} = \frac{C_L^2}{\pi \cdot \mathrm{AR}} \tag{23}$$

$$C_f = \frac{0.075}{(\log(Rn) - 2)^2} \tag{24}$$

$$C_{DP} = \frac{C_f \cdot \mathrm{S}_w \cdot 1.1}{A} \tag{25}$$

$$C_{D,tot} = C_{DP} + C_{DI} \tag{26}$$

$$C_{D,exp} = \frac{D}{1/2 \cdot \rho \cdot \mathrm{V}^2 \cdot \mathrm{A}} \tag{27}$$

$$C_{L,exp} = \frac{L}{1/2 \cdot \rho \cdot \mathrm{V}^2 \cdot \mathrm{A}} \tag{28}$$

$C_{D,exp}$ and $C_{L,exp}$ are the experimental coefficients from the wind tunnel tests. The $C_{L,2D}$ used in Prandtl's method for calculating the lift coefficient is the lift coefficient per degree in the two-dimensional case. C_{DP} and C_{DI} are the frictional drag respectively the induced pressure drag which are used to calculate the total theoretical drag $C_{D,tot}$. In appendix A these coefficients can be seen plotted against angle of attack for all keels.

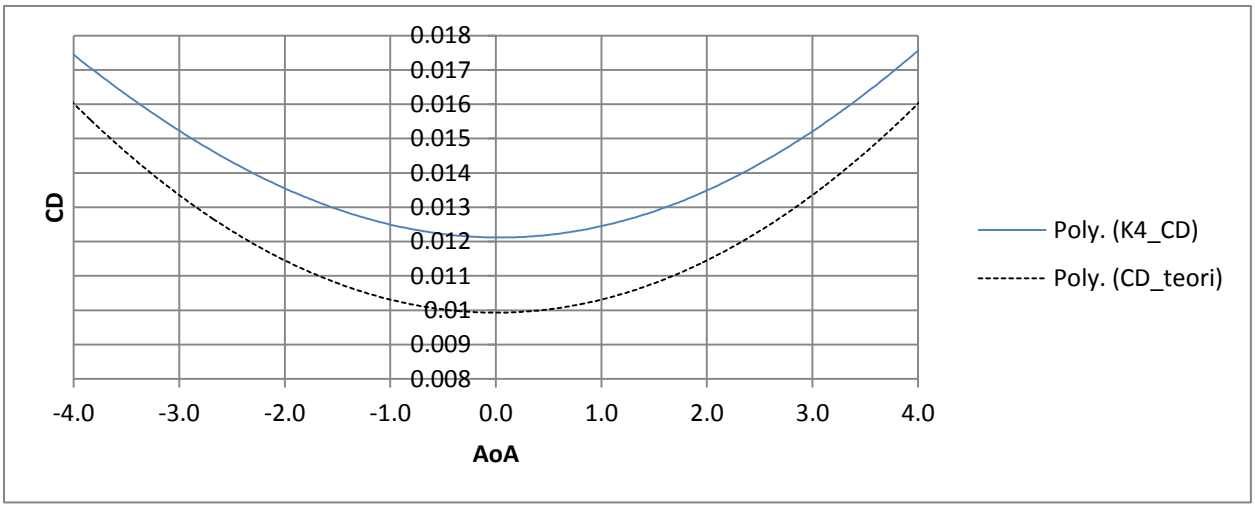

Figure 46: C_D from theory compared to experimental value

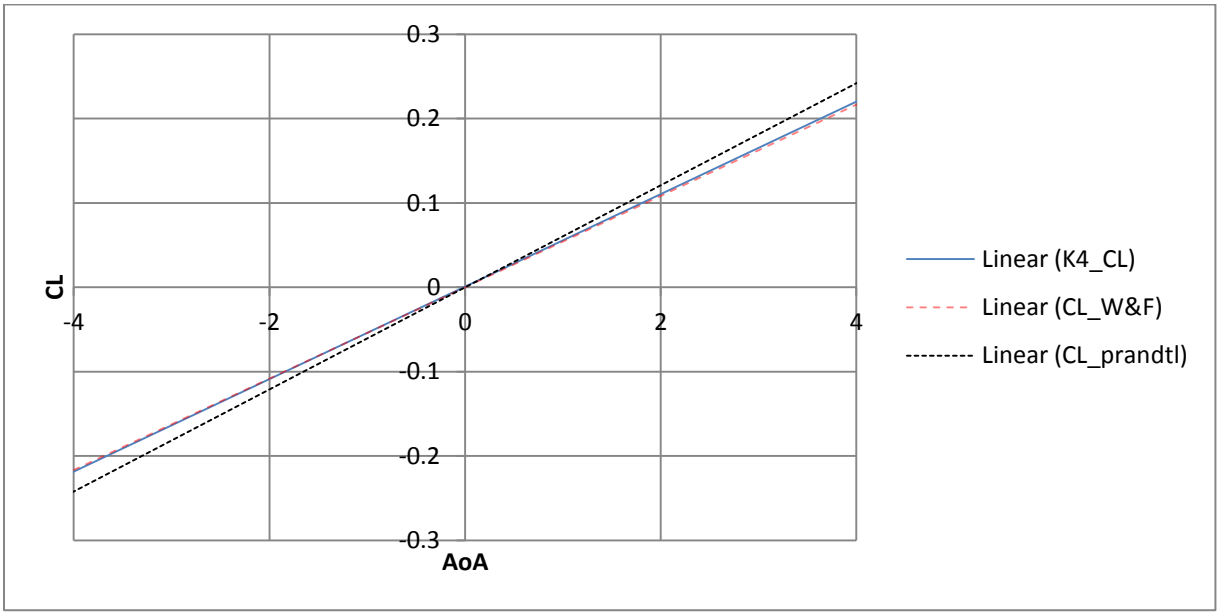

Figure 47: C_L from theory compared to experimental value

In Figure 46 the theoretical total drag $C_{D,\ tot}$ is found to be approximately 10% lower than the experimental values. As seen in Appendix A, this difference is smaller for keel 1 than for the other keels. One reason is that the theoretical values are calculated using the reference values of keel. A difference was however expected since a real case is seldom represented by the theory with higher precision.

In Figure 47 the experimental C_L and $C_{LW\&F}$ from Whicker and Fehlner's report coincides very well. The C_L from Prandtl's formula over predicts the lift curve.

Both Prandtl's and Whicker and Fehlner's formula for C_L are based on a wing without a bulb. Prandtl's formula is also designed for AR > 4, which is not the case for the different keel designs in this report. Despite this both theories coincides very well but it is not possible to explain why Whicker and Fehlner's C_L is so close to the experiment data and Prandtl's differs a bit.

All measured data for every keel was input to graphs, and the trend line function in Excel was used to get the average curves. Before the trend line function was used, a normal scatter of measurement values looked like in Figure 48 and Figure 49. Note that the measurements origins from three separate measurement series, and have been corrected according to above mentioned corrections.

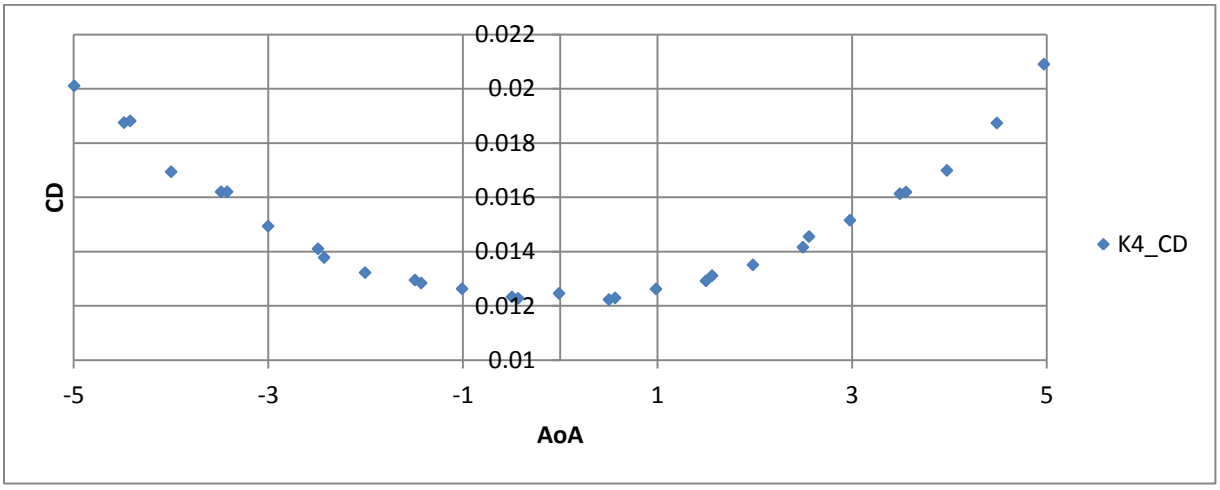

Figure 48: Scatter of CD values

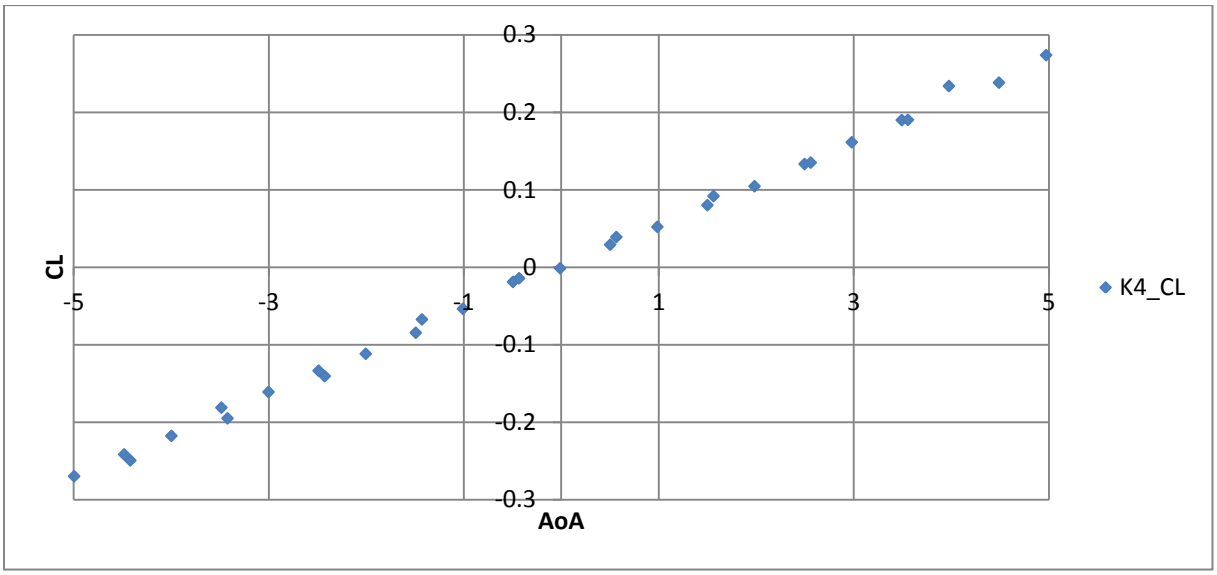

Figure 49: Scatter of CL values

Comparison between K1-K4

In this part results from wind tunnel testing are presented only compared between the keels. This, as mentioned, gives a good comparison of the trends as all keels are assumed to share the same bias errors.

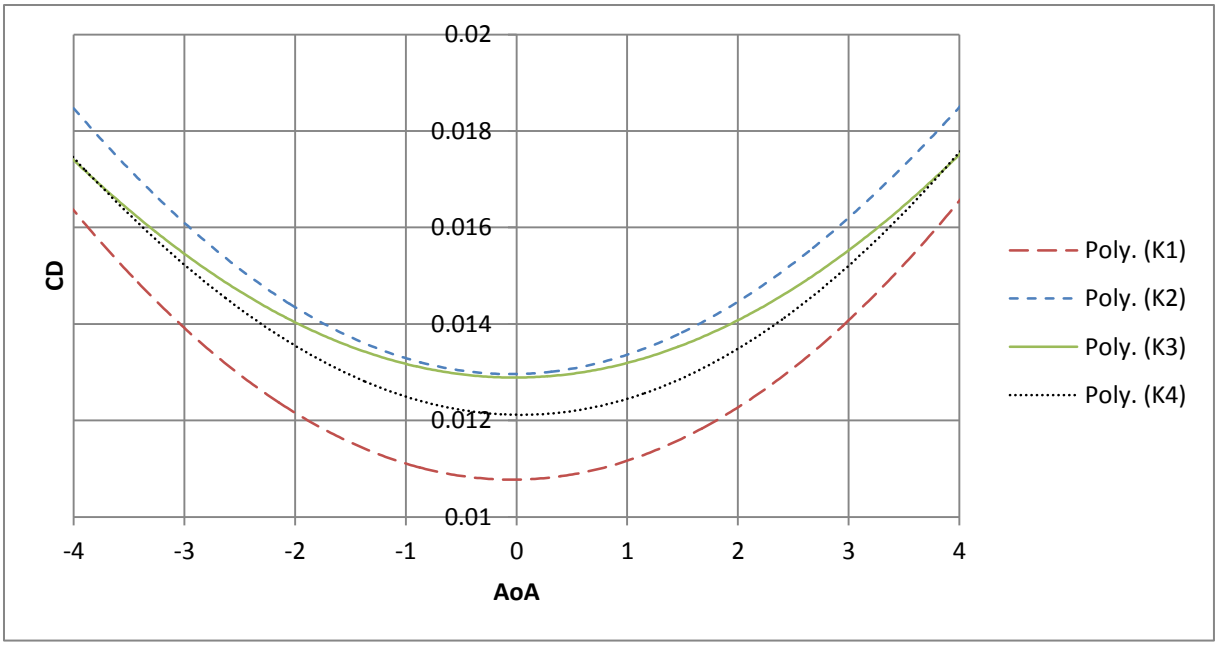

Figure 50: Comparison of C_D between K1-K4

As can be seen in the graph, of the bulb keels, keel 4 has lowest drag at zero angle of attack. It increases faster than keel 3, which means that at 4° angle of attack keel 3 and 4 have equally large drag forces. Keel 1 was as expected best performing, but it was only evaluated as reference.

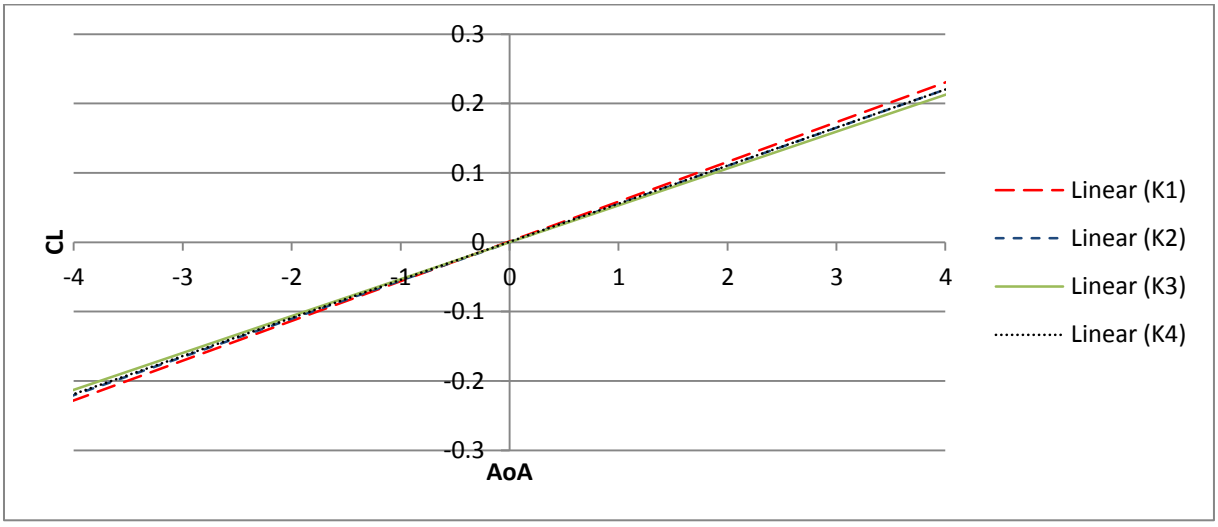

Figure 51: Comparison of C_L between K1-K4

Keel 4 has according to the graph best lift curve compared to keel 2 and 3. Keel 1 has best lift because of its larger effective area, and keel 3 has lowest lift curve. In Table 6 some values from the graphs can be found.

Table 6: C_D and C_L in numbers

	CD			CL		
AoA	0°	2°	4°	0°	2°	4°
K1	0.0108	0.0122	0.0165	0	0.115	0.228
K2	0.0130	0.0144	0.0185	0	0.110	0.222
K3	0.0129	0.0140	0.0175	0	0.108	0.213
K4	0.0121	0.0135	0.0175	0	0.110	0.223

Figure 50 describes the most important behaviour and performance of the keels: the relationship between lift and drag forces. From the graph any given lift can be set, and a corresponding drag can be read. It can clearly be found that keel 4 is the better performing one of the bulb keels; especially at small angles of attack. At larger angles of attack the trends from this curve, and more specifically from Figure 46, keel 3 is the best performing keel. This however only for very large angles of attack, for more reasonable angles of attack keel 4 is the best performing bulb keel. It is quite clear that keel 2 is inferior to the others at all lift coefficients measured.

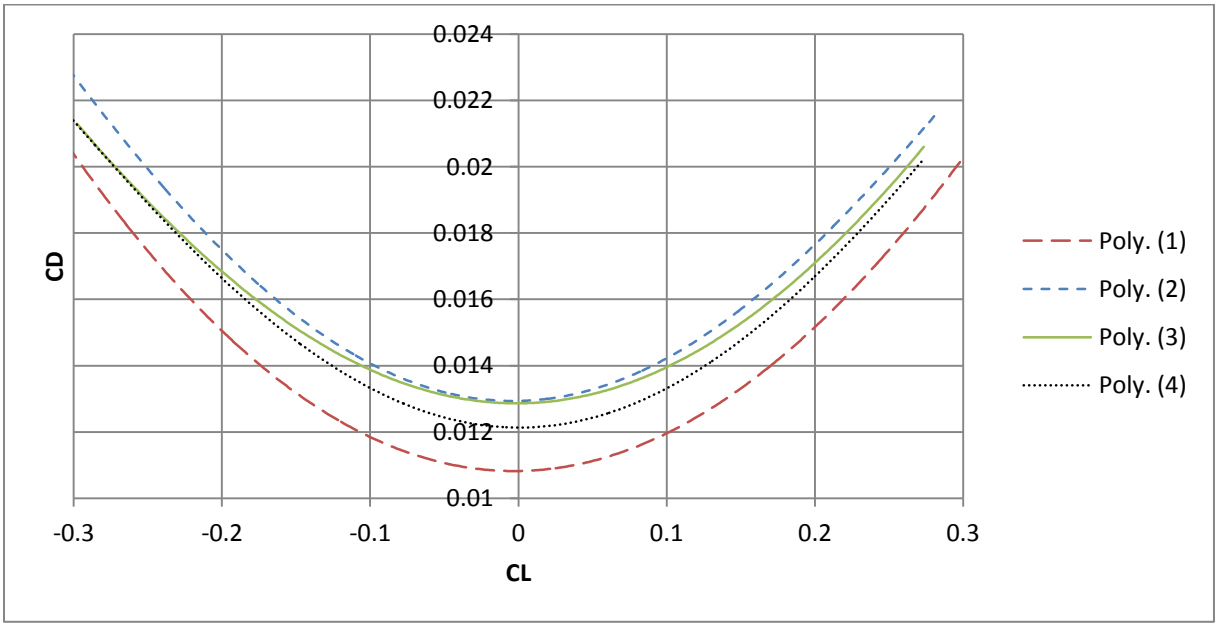

Figure 52: C_L as function of C_D

The curve in Figure 52 is the most sensitive way of interpreting the results since it depends on the uncertainties squared, and although effort has been put in minimizing the uncertainties an unsymmetric behaviour can be seen.

A comparison between the wind tunnel and CFD results for each keel is presented in the Results part on page 35.

3.2.7 Discussion

As can be realized from the previous part there are many aspects and which needs to be fulfilled while performing wind tunnel tests. The un-symmetry in Figure 52 should not be too worrying as this curve depends on the uncertainties squared. Over all, satisfactory results and measurements have been gained. Further discussion and a comparison between results gained from wind tunnel tests and CFD can be found in the global results and discussion on page 40 and 42.

3.3 VPP

To evaluate the keels in a more quantitative way the VPP program WinDesign was used. The aim of the VPP was to get a comparable result between the keels that was easier to interpret than the theoretical coefficients gained directly from CFD and wind tunnel testing.

For the VPP, an Olympic court was input as route, and the performance of the keels was quantified by calculating the time the YD 40 [1] needed to complete the race, with each different keel mounted.

3.3.1 Introduction

Velocity prediction programs are used to predict the velocity of a sailing yacht. The program formulates the equilibrium behaviour of the yacht as a set of nonlinear equations summarizing forces and moments on the yacht. The program requires models for both the hydrodynamic forces on the hull and the aerodynamic forces on the sails. In Figure 53the different forces acting on the yacht are shown. These are used in the VPP program to calculate the velocity at different wind speeds and angles. The results were intended to be a compliment to the CFD results and to give a more straight forward result.

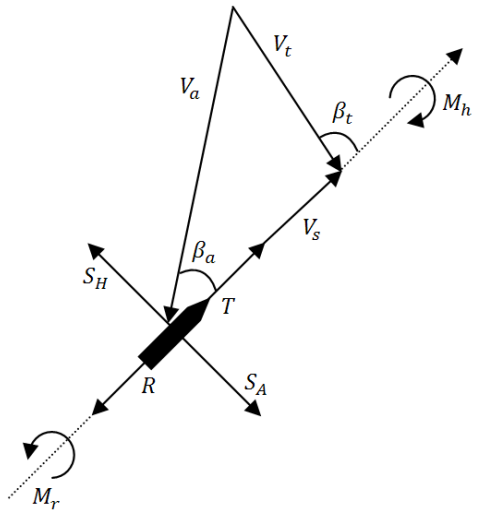

M_r– Roll moment
R – Resistance
T – Thrust
S_A – Aero dynamic side force
S_H – Hydro dynamic side force
V_s – Ship speed
V_a – Apparent wind speed
V_t – True wind speed
β_a – Apparent wind angle
β_t – True wind angle
M_h – Heeling moment

Figure 53: Forces on the yacht, [19]

3.3.2 Configurations

First, hydrostatic calculations for the YD-40 [1] hull with the different keels were made. The program used for this was Rhino. All the keels were placed with their maximum pressure at the same longitudinal position on the hull. It was assumed that no heel or trim occurs for either of the keels in start position. Drawing of the YD-40 can be seen in Figure 54.

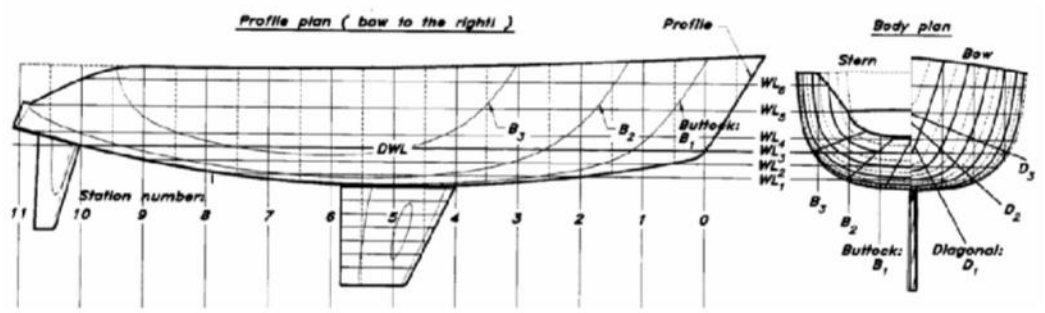

Figure 54: Drawing of the YD-40 [1] by permission by the author

Main Dimension of the YD-40:

- Overall length: 12.05 [m]
- Waterline length: 10.02 [m]
- Maximum width: 3.71 [m]
- Hull depth: 0.57 [m]
- Displacement without keel: 4870 [kg]

The results from Rhino were incorporated into WinDesign for VPP evaluation. Data inputted in the VPP are hydrostatics for the hull and C_L and C_D for the keels measured in the wind tunnel. Automatic functions in the program were used to generate the sail sets and other values necessary. The aim of the VPP was as mentioned to be able to compare the different keel designs and therefore all values not associated with the keels where kept constant; therefore, the automatic functions could be used. There is no possibility to directly import C_L and C_D in the VPP program WinDesign so instead the program was manipulated a bit and the effective draft for the keels was used instead of the maximum draft. From the wind tunnel the drag coefficient for zero angle of attack was known.

$$C_{D0} = profiledrag + frictiondrag \tag{29}$$

It was assumed that C_{D0} could be expressed with the following constant value:

$$C_{D0} = (1 + k)C_f \tag{30}$$

where C_f is calculated with the ITTC rule [6] as in equation (24). The constant k is calculated for each keel and used together with the wetted surface from keel 1 to scale the wetted surface for the bulb keels.

$$S_{Wi} = \frac{(1 + k_i)}{(1 + k_1)} S_{w1} \tag{31}$$

The total drag coefficient is equal to:

$$C_D = C_{DI} + C_{D0} \tag{32}$$

where C_{DI} is the induced drag. From the induced drag and the lift coefficient the aspect ratio AR can be calculated [1]:

$$C_{DI} = \frac{C_L^2}{\pi \cdot AR} \tag{33}$$

According to Orych [20] the aspect ratio can be used to calculate the effective draft T_e:

$$T_e = \sqrt{\frac{S \cdot AR}{2}} \tag{34}$$

S is the plan form area of the keel. The C_L and C_D where incorporated to WinDesign through the scaled wetted surface and the effective draft.

3.3.3 Evaluation of performance

The aim of the investigation was to evaluate the upwind performance for four different keel designs. Table 7 shows the max velocity for the different keels upwind for a constant wind speed of 16 knots.

Table 7: Different velocities for upwind performance with constant true wind speed of 16 knots

Angle of attack	K1	K2	K3	K4
32	6.881	6.868	6.883	6.883
40	7.342	7.337	7.345	7.348
60	7.999	8.008	8.011	8.016
90	8.447	8.48	8.483	8.492
120	7.942	7.953	7.954	7.963

As can be seen in Table 7 the results between the keels are very even. Keel 1 has no bulb and that makes it not comparable to the keels with bulbs. During the VPP keel 1 has only been used as a reference. Between the bulb keels, keel 4 is the winner; it has a higher velocity at all wind directions than both keel 2 and keel 3. The Keel with the worst performance is keel 2; but it is very close between the last two bulb keels.

Polar plot is a very helpful tool when the performance for all different wind speed and wind directions is to be evaluated. It is not possible to see the differences between the keels in a polar plot due to the fact that the results were so close to each other as shown in Table 7. Thereby only the polar plot from keel 4 is included in Figure 55. The wind speed varies between 4 and 25 knots, the wind direction between 0 and 180 degrees and the boat velocity goes up to almost 10 knots.

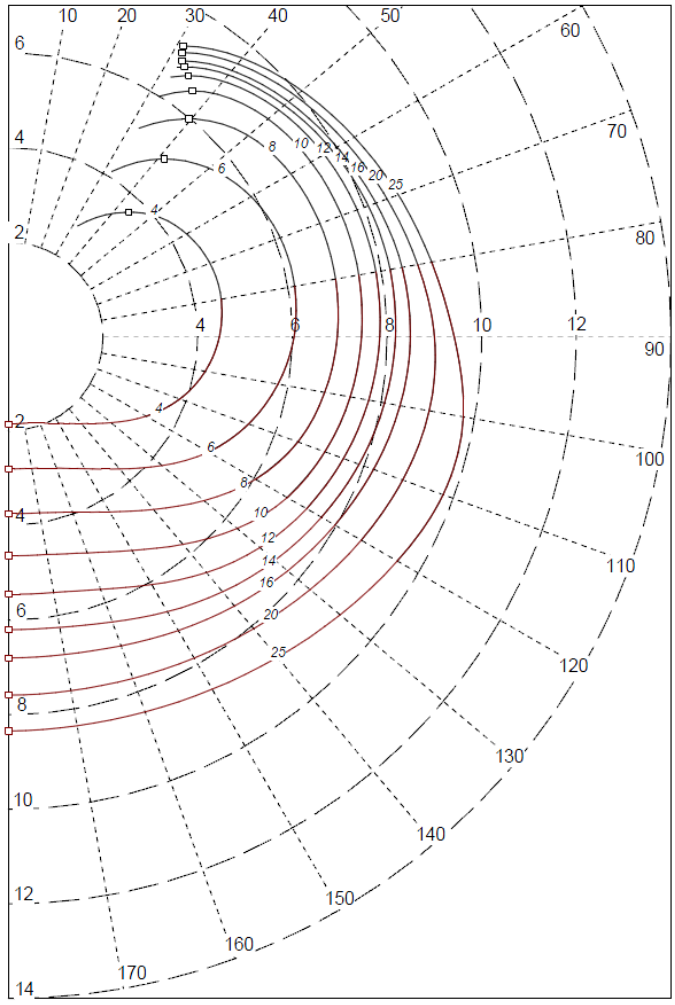

Figure 55: Polar plot, keel 4

The downwind performance is very low for all the keels. One reason for this can be that the same sail set was used for all wind directions; if a downwind sail, like a spinnaker, had been used it had probably given a higher result downwind. Since mostly the upwind performance was of interest for this evaluation the automatic sail set with only a main sail and a jib was used.

The keels were also evaluated against each other on a race. The results from ten nautical miles on an Olympic track are presented in Table 8. Four different wind speeds have been chosen and the time is presented in minutes.

Table 8: Results for the Olympic race in minutes:

True wind speed (kn)	**K1**	**K2**	**K3**	**K4**
8	145.10	145.99	145.88	145.31
12	109.40	109.74	109.61	109.42
16	95.63	95.78	95.67	95.59
20	89.57	89.63	89.53	89.50

The times for completing the race are extremely similar. Keel 4 has the lowest lap time for the different true wind speeds. What's most interesting is that at low true wind speeds keel 4 is even faster that keel 1.

4 Comparison between CFD and Wind tunnel Data

In this part hard numbers of C_D and C_L are presented for comparison between CFD and wind tunnel tests. In Table 9 and Table 10 these coefficients non-dimensionalised by A_L of keel 1 can be seen.

Table 9: C_L from Wind Tunnel tests and CFD

C_L	K1	K2	K3	K4
Wind Tunnel	0.228	0.222	0.213	0.223
CFD	0.253	0.252	0.246	0.241
Difference	10%	12%	13%	7%

Table 10: C_D from Wind Tunnel tests and CFD

C_D	K1	K2	K3	K4
Wind Tunnel	0.0165	0.0185	0.0175	0.0175
CFD	0.0170	0.0197	0.0189	0.0183
Difference	3%	6%	7%	4%

Table 11: C_L/C_D for both Wind Tunnel tests and CFD

C_L/C_D	K1	K2	K3	K4
Wind Tunnel	13.82	12.00	12.17	12.74
CFD	14.85	12.83	13.03	13.18
Difference	7%	6%	7%	3%

From these tables it can be concluded that the wind tunnel results are up to 13% smaller than the CFD results for C_L and up to 7% for C_D. The comparison C_L/C_D is up to 7% smaller for the wind tunnel. The ranking of the C_L/C_D results is the same in CFD as in the tunnel.

For explaining the difference between the wind tunnel and CFD results both the uncertainties in CFD and the experiments will have to be evaluated. Thus, when none of the performed grid variation studies worked for the used grids no validation error was gained for the CFD. This resulted in that no comparison could be made between the comparison error, E, with the total uncertainty, U_{TOT}, which consist of the validation error, U_{VAL}, together with the numerical error, U_{SN}, and the measurement error U_D.

The main reason for the difference in values is thought to be a result of that the CFD calculates with a turbulent flow for the whole model whereas the flow on the model upstream

from the tape in the wind tunnel is laminar. Also a difference could have been introduced when doing the tripping of the flow when as mentioned a continuous taping was chosen before an exact similarity between the keels; this was however not expected to be a major reason.

Another source for the difference can be found in the CFD. Since all the forces are overestimated in the CFD, it may be that the solver has calculated the flow with a too low R_n. There was some ambiguity in the definition of the Reynolds number, which was not fully clarified.

Also differences between the meshes might have occurred when the keels shape differences made them difficult to mesh exactly similarly.

5 Discussion

As the fin keel only was set to be a reference to the other keels, not so much attention has been given to its performance. As can be noticed, it has superior performance in low wind speeds because of its smaller wetted surface and larger chord length. However, to get the same properties designing it to be made of cast iron, it would be unreasonably large. It would also be much heavier than the bulbed keels due to its higher centre of gravity.

In higher wind speeds the T-keel performs better than the fin keel when it has larger righting moment. Also the integrated L-bulbed keel has its characteristics with a high righting moment and a higher lift force due to the gradual thickening of the profile, and with a proper optimization of this keel type some advantage might be gained.

It is very hard to say which basic keel type that is best suitable for a yacht in an over-all performance point of view. In our case a T-bulbed keel was found to be the best performing one, but for other yacht designs this might not be true. Some aspects that should be taken into account are as follows; some were mentioned in the introduction part.

- **Intended Yacht type and hull:** for an ocean crossing yacht a T-bulbed keel might be unpractical due to the risk of nets and lines getting stuck whereas a racing yacht needs a T-keel for the required righting arm
- **Position of LCE and LCG:** for a T-bulbed keel the LCE of the fin can be placed in an optimum position and then the LCG of the bulb can be placed separately whereas for the L-bulbed designs a balance between these two has to be found
- **Required righting arm:** in upwind sailing when a high righting arm is required a bulbed keel is preferred whereas in downwind sailing a low wetted surface is more important
- **Maximum draft:** for practical reasons as entering harbours a low draft is better, for achieving the required righting arm a bulbed keel might be needed
- **Customer requirements:** the reason for that the T-keels have become so popular might be that it is a trend, and that the racing yachts seen on different competitions mostly uses T-keels

When having decided which basic design that should be used, this should then be hydro dynamically optimised with the constraints from the above definitions for gaining the best over-all performance.

6 Conclusions

The Aim of this Master's Thesis was to identify which of the chosen basic keel designs that has the best performance upwind, both evaluated alone in a wind tunnel domain using CFD and wind tunnel tests and together with a hull using VPP. The results as analyzed throughout chapter 3 to 5 has consistently shown that for both these cases the T-bulbed keel performs best of the bulbed keels, and also better than the fin keel in higher wind speeds.

Another aim was to determine whether a proper design of one of the basic design types could change the outcome of the comparison. When the T-bulbed keel was completely redesigned after its poor performance from the Bachelor's Thesis [2], and this new design proved to be the best performing one this aim was definitely answered.

Finally the results from the wind tunnel were found to be of a high order of accuracy, and as stated in the Aim and Objectives will be open for further validation of the keels using other CFD software and theories.

7 Further work

For further work some main topics can be mentioned. Firstly, we gained a lot of experience using the wind tunnel, and an experienced wind tunnel operator with a different set-up might gain a higher order of accuracy.

For the CFD part it might be an interesting opportunity to perform potential flow calculations to compare with the RANS calculations run here. When computational time becomes cheaper and computers more powerful there is also definitely an opportunity to run LES calculations for comparison.

In general the keels performed well. One possibility in a future thesis would be to first optimize all keels with the same optimization aspects, and then do a similar comparison as have been done here in order to know a “good” integrated L-keel is compared with a “good” T-keel etc.

For future wind tunnel tests there is definitely an opportunity to mount wings on either of the bulb keels, preferably the T-keel which performed best, and see if winglets could decrease the vortices even more.

An easy and possibly very beneficial continuation of this thesis can also be made by using the hydrodynamic coefficients and inputting them in a VPP while varying the material of the keels, and hence gain results for all the different keels with different manufacturing techniques.

8 References

1. **Larsson, Lars and Eliasson, Rolf E.** *Principles of Yacht Design.* s.l. : International Marine/McGraw-Hill, 2007. Vol. III.

2. **Bergman, Emil, et al.** *BSc. Investigation of Keel Bulbs For Sailing Yachts.* Göteborg : Chalmers University of Technology, 2010.

3. **Axfors, Björn, et al.** *ARC 45 Performance Cruiser.* Göteborg : Chalmers University of Technology, 2010.

4. **Ira H. Abbott, Albert E. Von Boenhoff.** *Theory of Wing Sections.* Toronto : General Publishing Company, 1958.

5. **Hepperle, Martin.** http://www.mh-aerotools.de/airfoils/javafoil.htm. [Online]

6. **Larsson, Lars and Raven, Hoyte C.** *Ship Resistance and Flow.* New Yersey : The Society of Naval Architects and Marine Engineers, 2010.

7. **FLOWTECH.** *XCHAP Theoretical Manual.* Göteborg : FLOWTECH, 2007.

8. —. *SHIPFLOW Users Manual.* Göteborg : FLOWTECH.

9. **Xing, Tao and Stern, Frederick.** Factors of Safety for Richardson Extrapolation. June 2010.

10. **Eça, L., Vaz, G. and Hoekstra, M.** A verifikation and validation exercise for the flow over a backward facing step. June 2010.

11. **Roache, P.J.** *Verification and Validation in Computational Science and Engineering.* 1998.

12. **Ljungqvist, Kasper.** *Shape Optimisation of an Integrated Bulb Keel.* Göteborg : Chalmers University of Technology, 2011.

13. **RUAG, Aerospace Defence Technology.** DNW: DMS–Waage 196–6H Kalibrierbericht zur Version C02. Emmen : s.n., 2004.

14. **Barlow, Jewel B., Pope, Alan and Rae, William H.** *Low-Speed wind tunnel testing.* s.l. : Wiley-Interscience, 1999. Vol. III.

15. **Werner, S.** *Computational Hydrodynamics Applied to an America's Cup Class Keel.* Gothenburg : Chalmers University of Technology, 2006.

16. **Ranzenbach, Robert and Zahn, Mathew.** *Experimental Methods to evaluate underwater appendages.* Annapolis, Maryland : The 17th Chesapeake sailing yacht symposium, 2005.

17. **Maskell, E.C.** *A Theory of the Blockage Effects on Bluff Bodies and Stalled Wings in a Closed Wind Tunnel.* London : Ministry of Aviation, 1963.

18. **FS-Equilibrium.** *FS-Equilibrium User manual.* 2010.

19. **Wallace, Stein W. and Ziemba, Willian T.** *Applications of Stochastic Programming.* Philadelphia : Society for Industrial and Applied Mathematics, 2005.

20. **Orych, Michał.** *Calculations of the flow and resistance components of systematically varied keel/bulb winglets in upright and heeled conditions.* Gothenburg : Chalmers University of Technology, 2005.

Appendix

A: Wind tunnel results

Keel 1

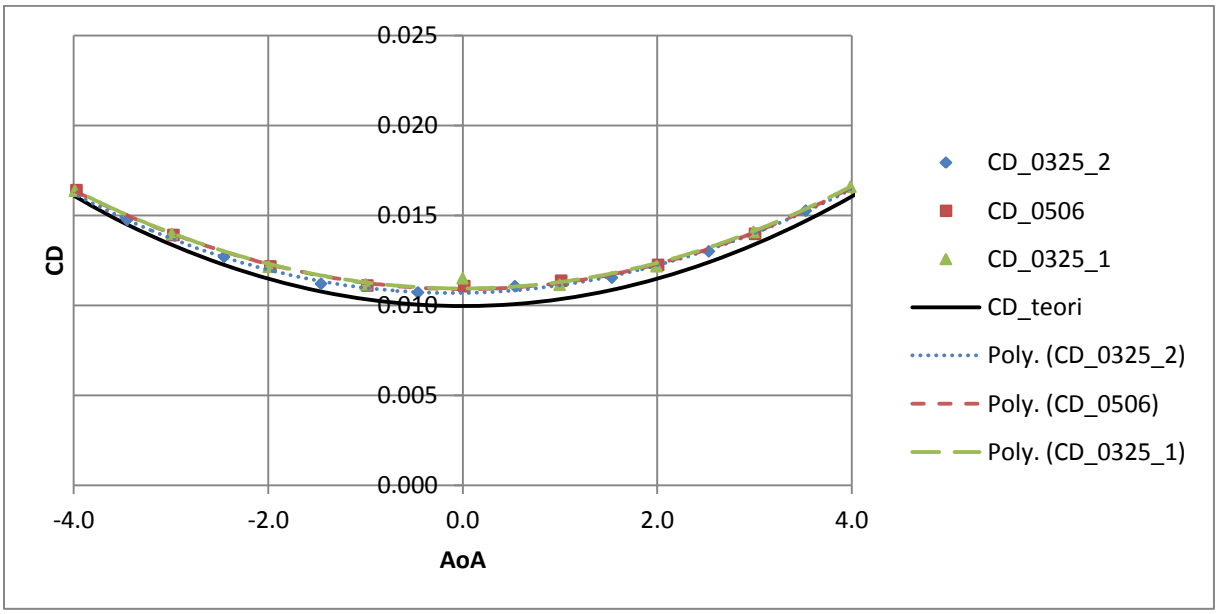

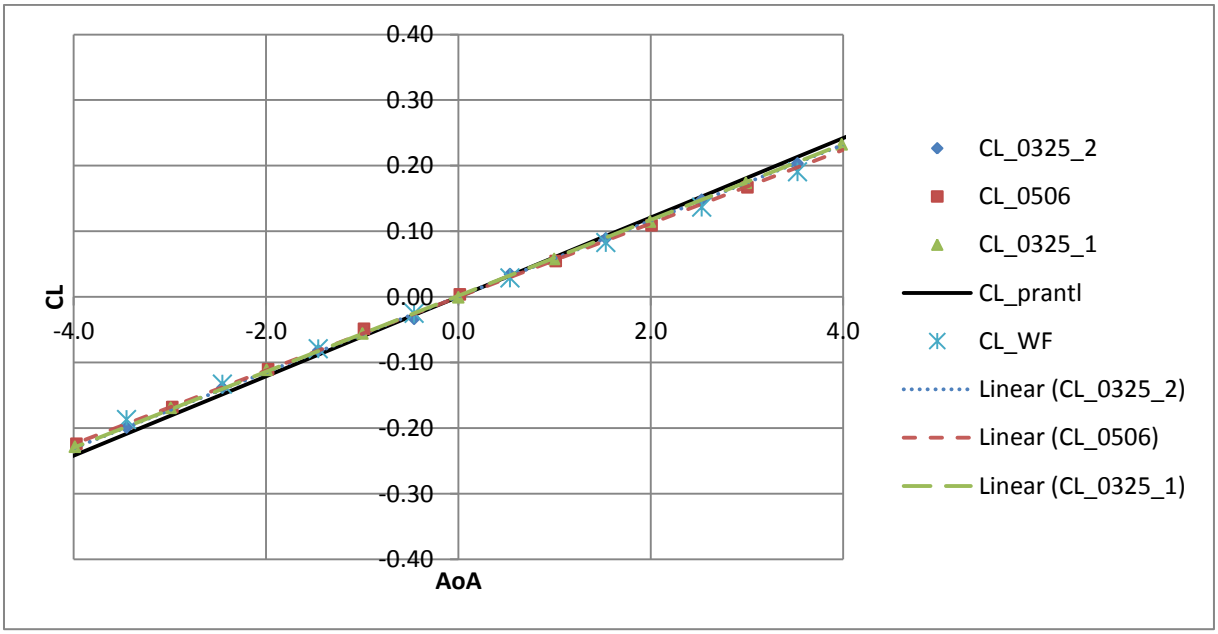

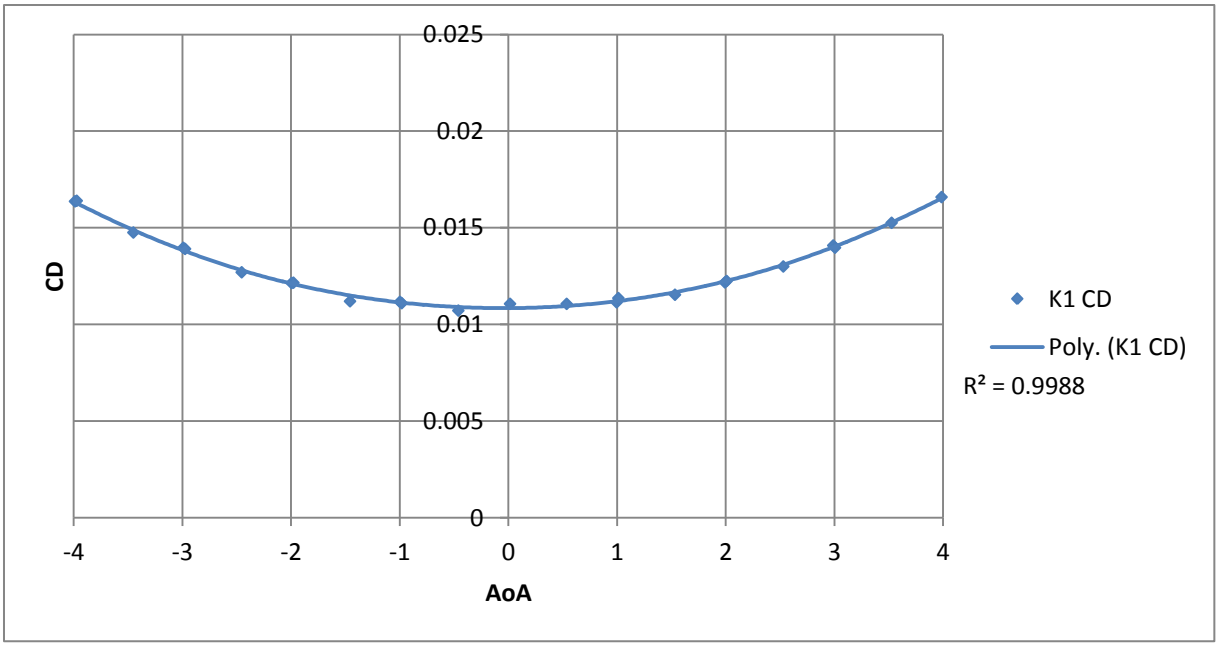
0.025
0.02
0.015
0.01
0.005
0
CD
-4
-3
-2
-1
0
1
2
3
4
AoA
K1 CD
Poly. (K1 CD)
R² = 0.9988

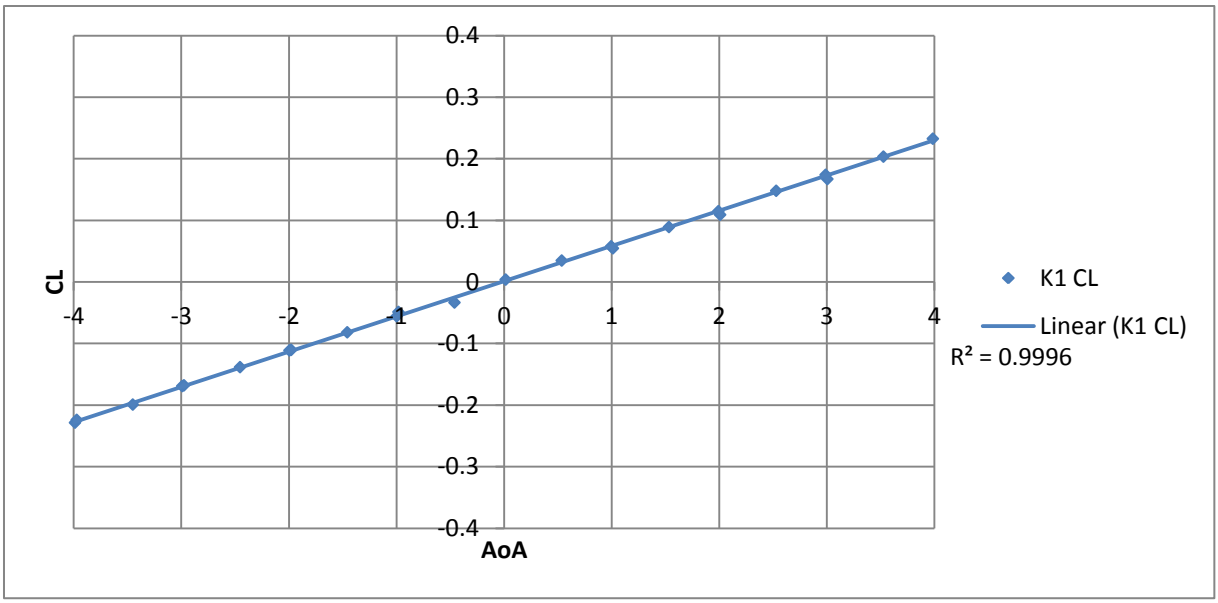
0.4
0.3
0.2
0.1
0
-0.1
-0.2
-0.3
-0.4
CL
-4
-3
-2
-1
0
1
2
3
4
AoA
K1 CL
Linear (K1 CL)
R² = 0.9996

Keel 2

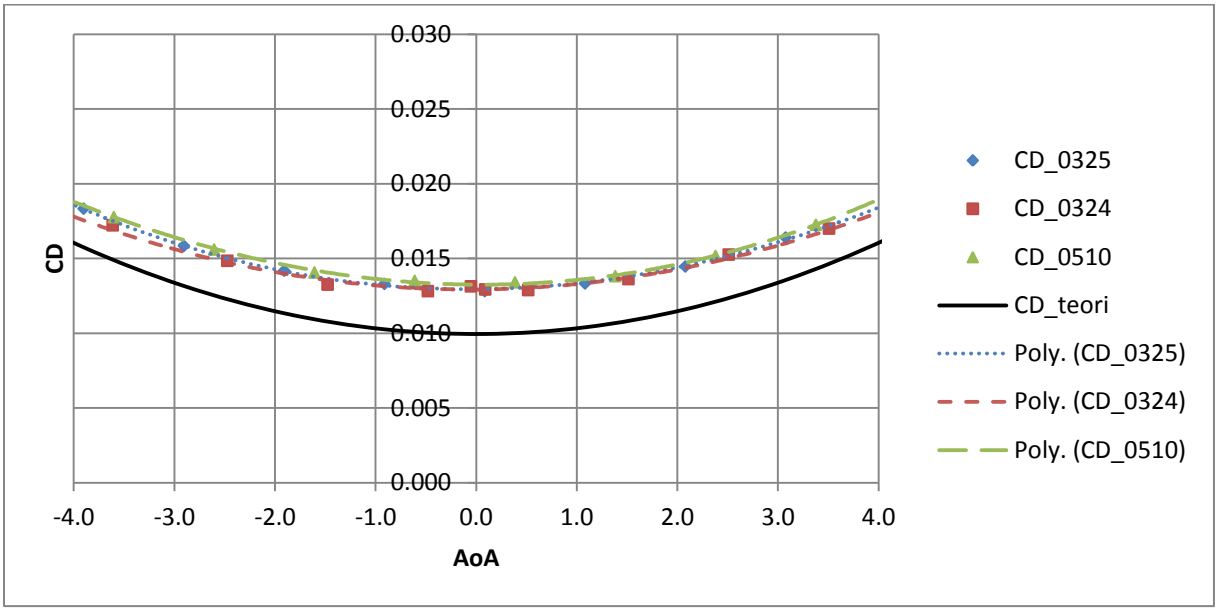
0.030
0.025
0.020
0.015
0.010
0.005
0.000
CD
-4.0
-3.0
-2.0
-1.0
0.0
1.0
2.0
3.0
4.0
AoA
CD_0325
CD_0324
CD_0510
CD_teori
Poly. (CD_0325)
Poly. (CD_0324)
Poly. (CD_0510)

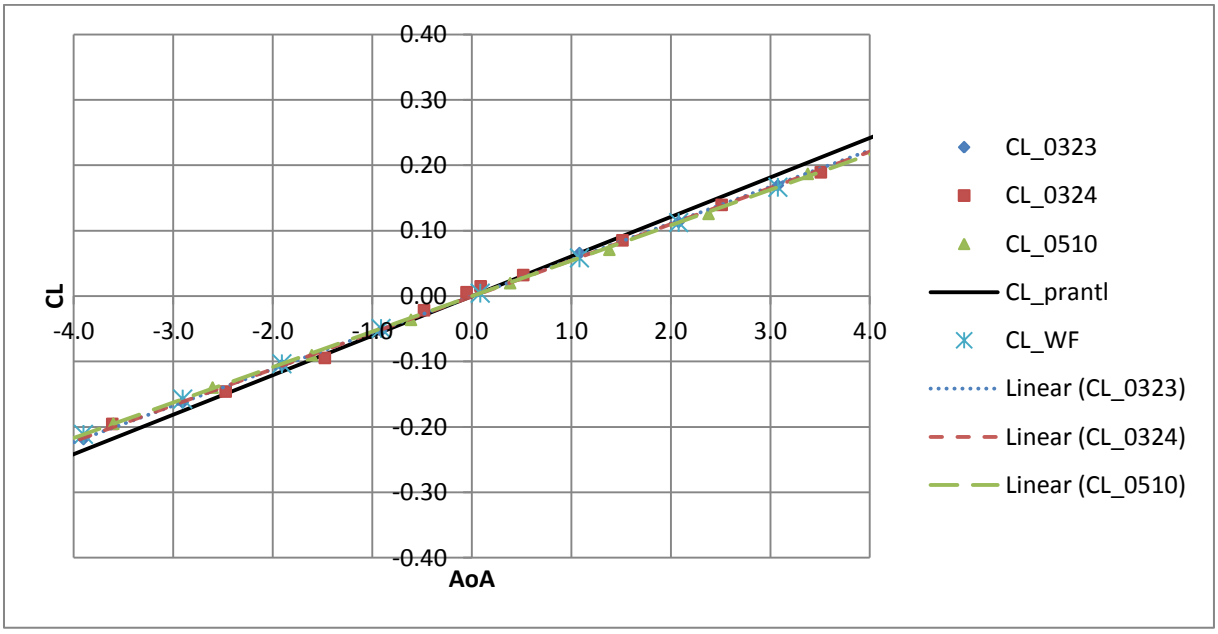
0.40
0.30
0.20
0.10
0.00
-0.10
-0.20
-0.30
-0.40
CL
-4.0
-3.0
-2.0
-1.0
0.0
1.0
2.0
3.0
4.0
AoA
CL_0323
CL_0324
CL_0510
CL_prantl
CL_WF
Linear (CL_0323)
Linear (CL_0324)
Linear (CL_0510)

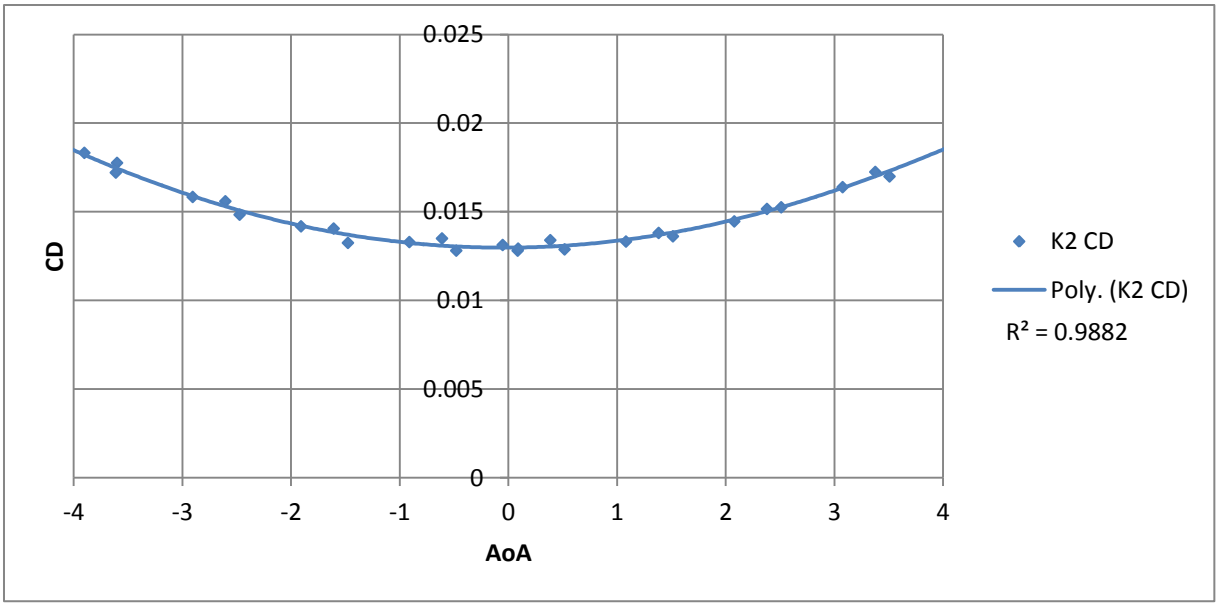
0.025
0.02
0.015
0.01
0.005
0
CD
-4
-3
-2
-1
0
1
2
3
4
AoA
K2 CD
Poly. (K2 CD)
R² = 0.9882

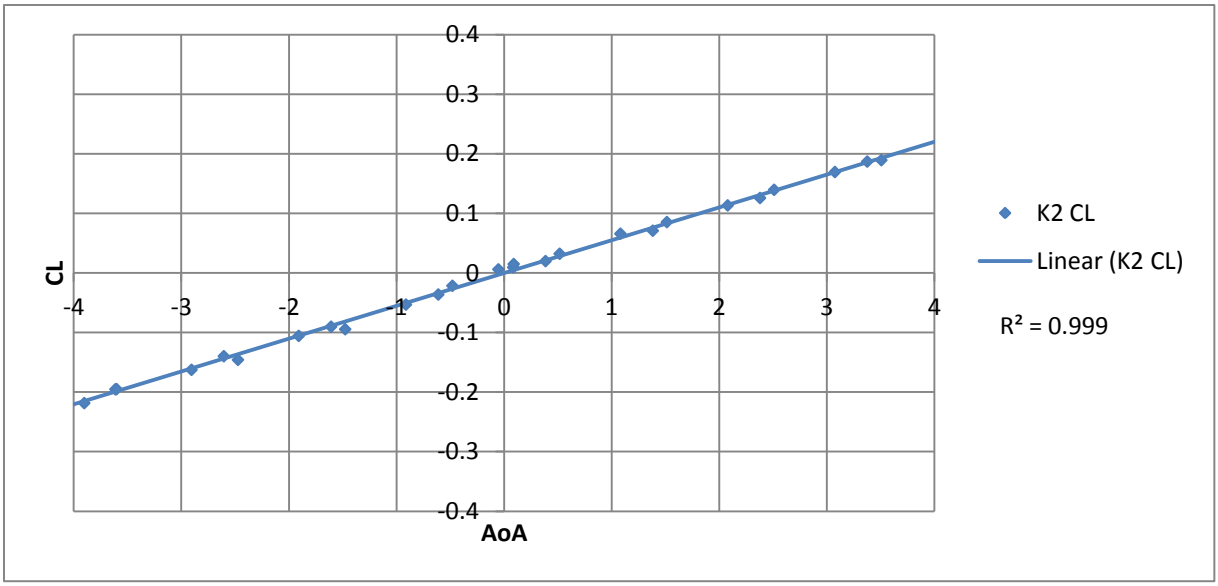
0.4
0.3
0.2
0.1
0
-0.1
-0.2
-0.3
-0.4
CL
-4
-3
-2
-1
0
1
2
3
4
AoA
K2 CL
Linear (K2 CL)
R² = 0.999

Keel 3

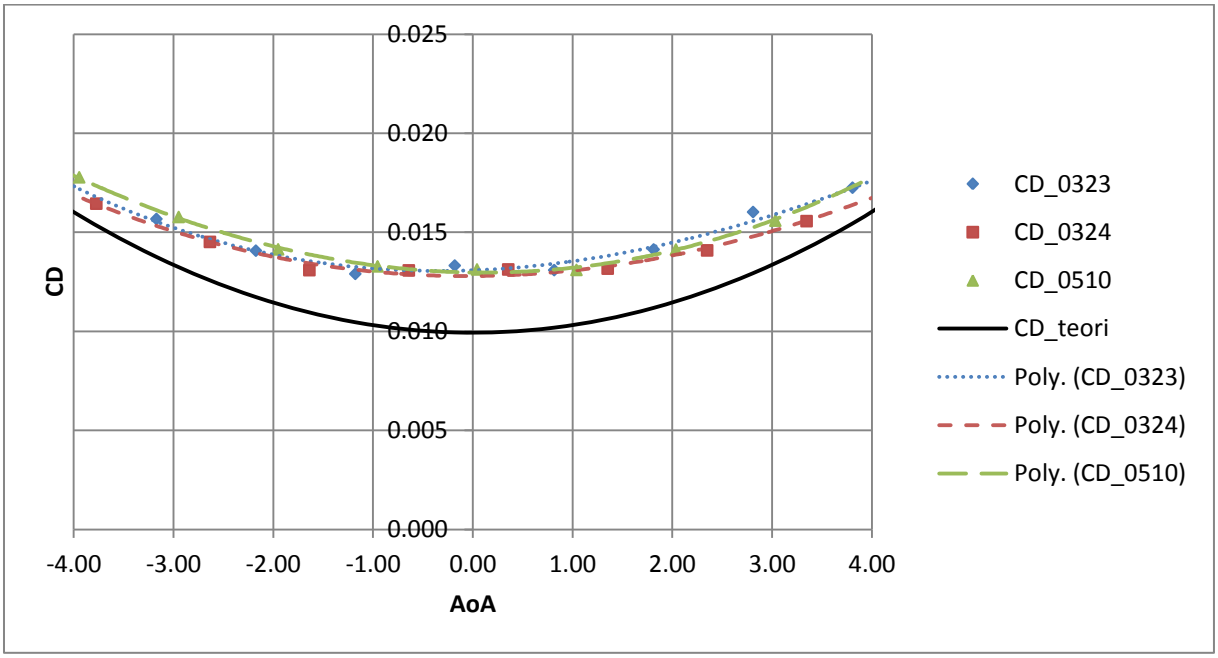
0.025
0.020
0.015
0.010
0.005
0.000
CD
-4.00
-3.00
-2.00
-1.00
0.00
1.00
2.00
3.00
4.00
AoA
CD_0323
CD_0324
CD_0510
CD_teori
Poly. (CD_0323)
Poly. (CD_0324)
Poly. (CD_0510)

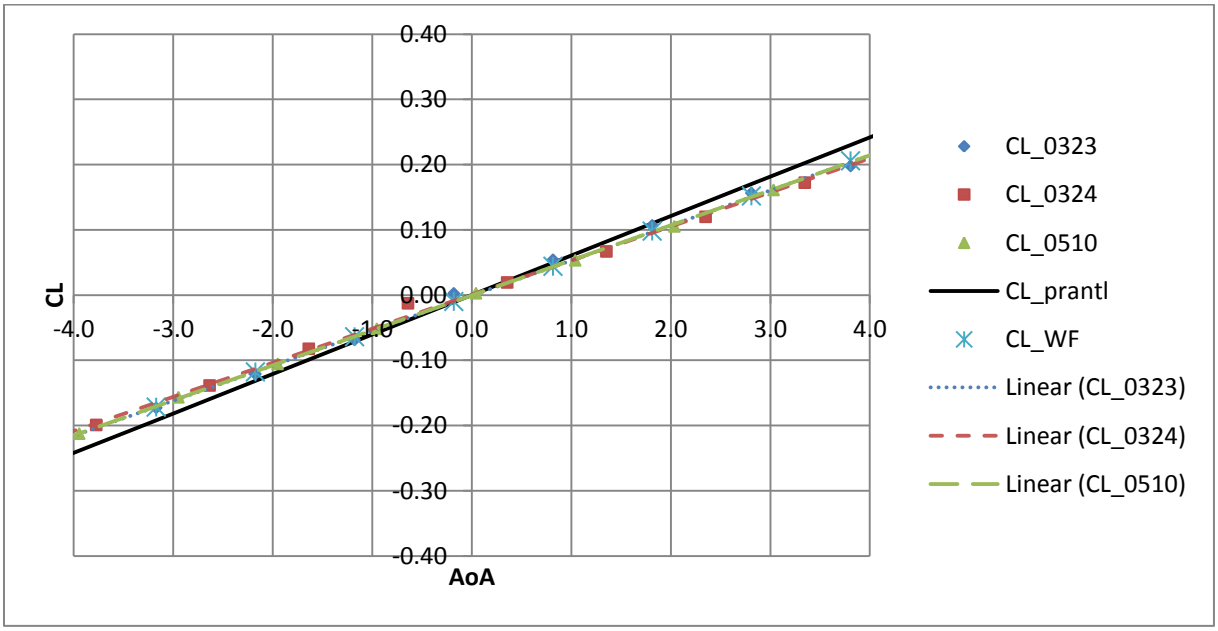
0.40
0.30
0.20
0.10
0.00
-0.10
-0.20
-0.30
-0.40
CL
-4.0
-3.0
-2.0
-1.0
0.0
1.0
2.0
3.0
4.0
AoA
CL_0323
CL_0324
CL_0510
CL_prantl
CL_WF
Linear (CL_0323)
Linear (CL_0324)
Linear (CL_0510)

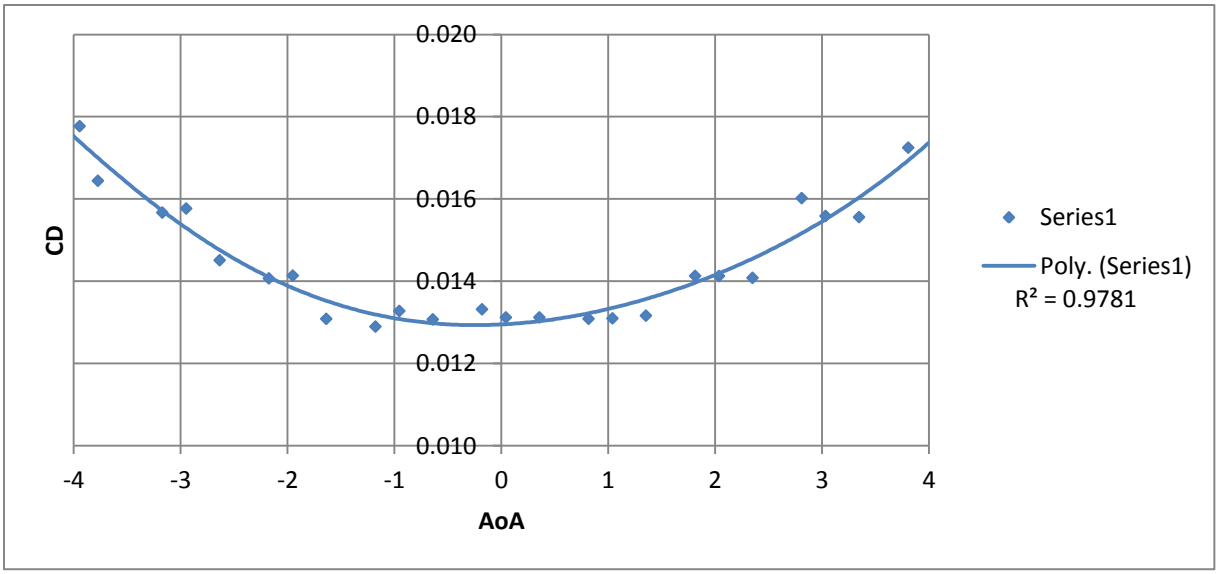
0.020
0.018
0.016
0.014
0.012
0.010
CD
-4
-3
-2
-1
0
1
2
3
4
AoA
Series1
Poly. (Series1)
R² = 0.9781

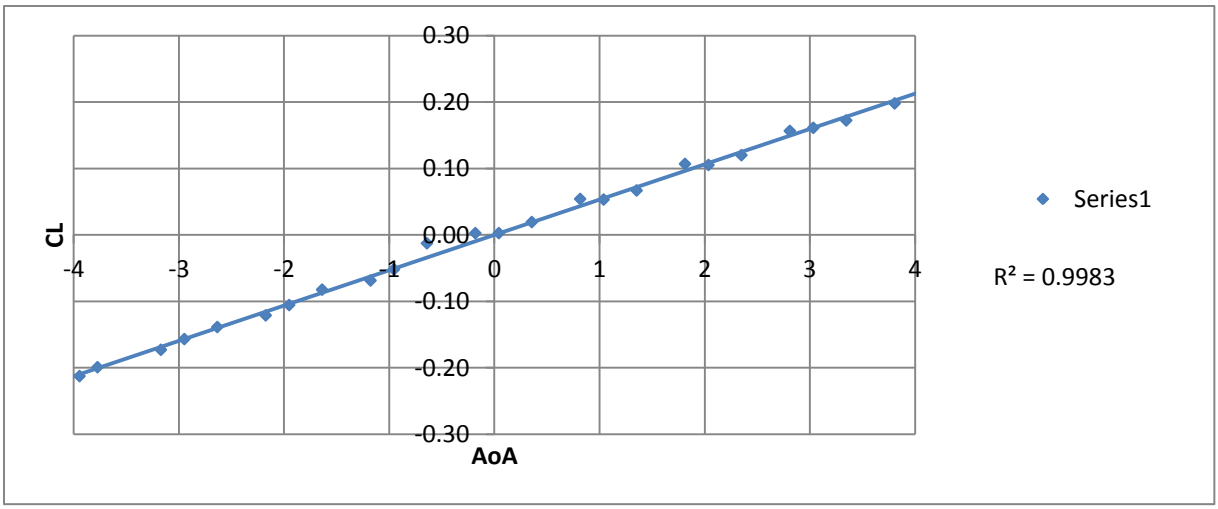
0.30
0.20
0.10
0.00
-0.10
-0.20
-0.30
CL
-4
-3
-2
-1
0
1
2
3
4
AoA
Series1
R² = 0.9983

Keel 4

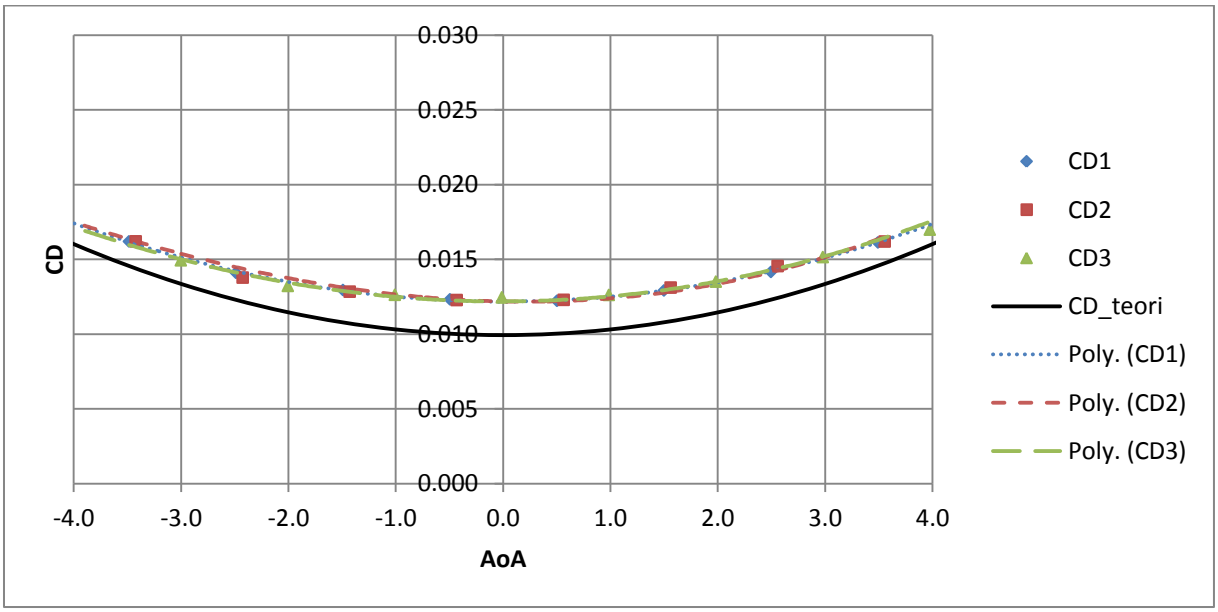
0.030
0.025
0.020
0.015
0.010
0.005
0.000
CD
-4.0
-3.0
-2.0
-1.0
0.0
1.0
2.0
3.0
4.0
AoA
CD1
CD2
CD3
CD_teori
Poly. (CD1)
Poly. (CD2)
Poly. (CD3)

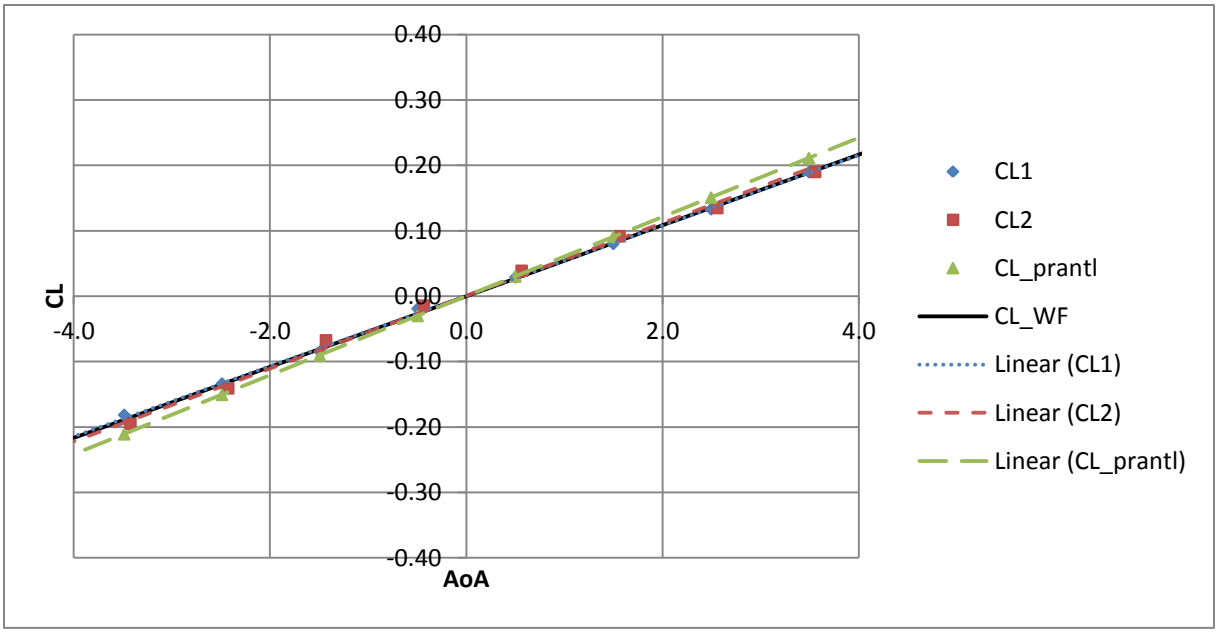
0.40
0.30
0.20
0.10
0.00
-0.10
-0.20
-0.30
-0.40
-4.0
-2.0
0.0
2.0
4.0
CL
AoA
CL1
CL2
CL_prantl
CL_WF
Linear (CL1)
Linear (CL2)
Linear (CL_prantl)

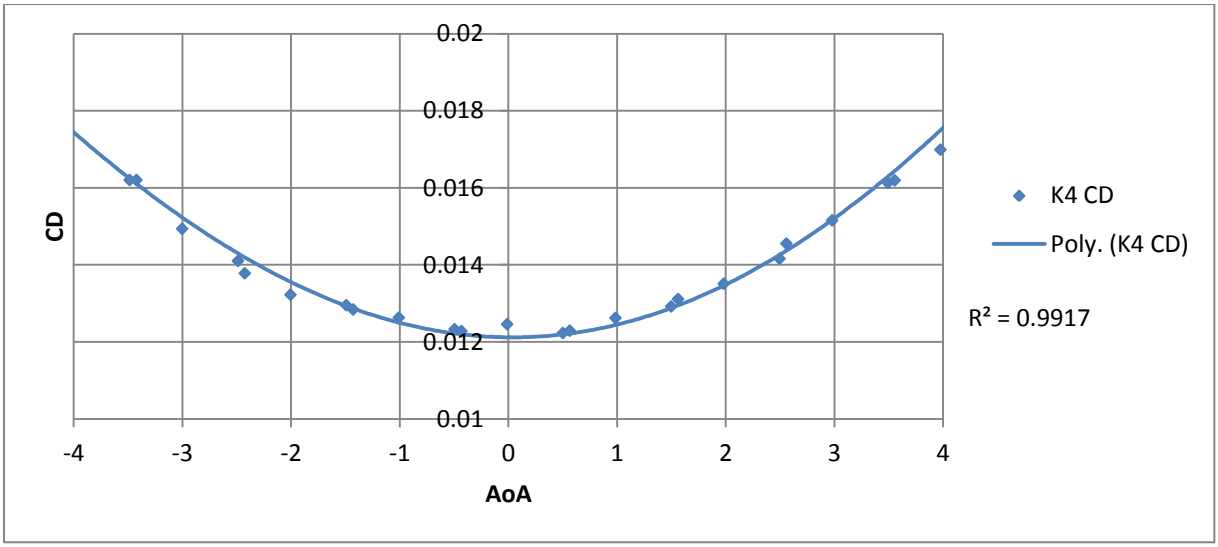
0.02
0.018
0.016
0.014
0.012
0.01
-4
-3
-2
-1
0
1
2
3
4
CD
AoA
K4 CD
Poly. (K4 CD)
R² = 0.9917

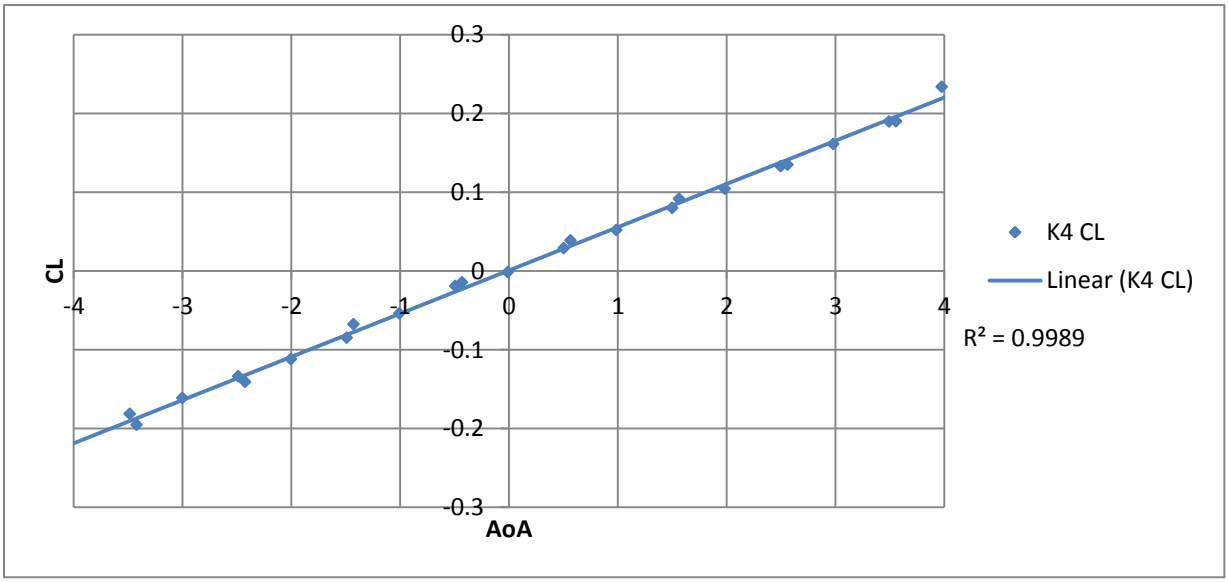
0.3
0.2
0.1
0
-0.1
-0.2
-0.3
-4
-3
-2
-1
0
1
2
3
4
CL
AoA
K4 CL
Linear (K4 CL)
R² = 0.9989

B: Keel Designs, perspective

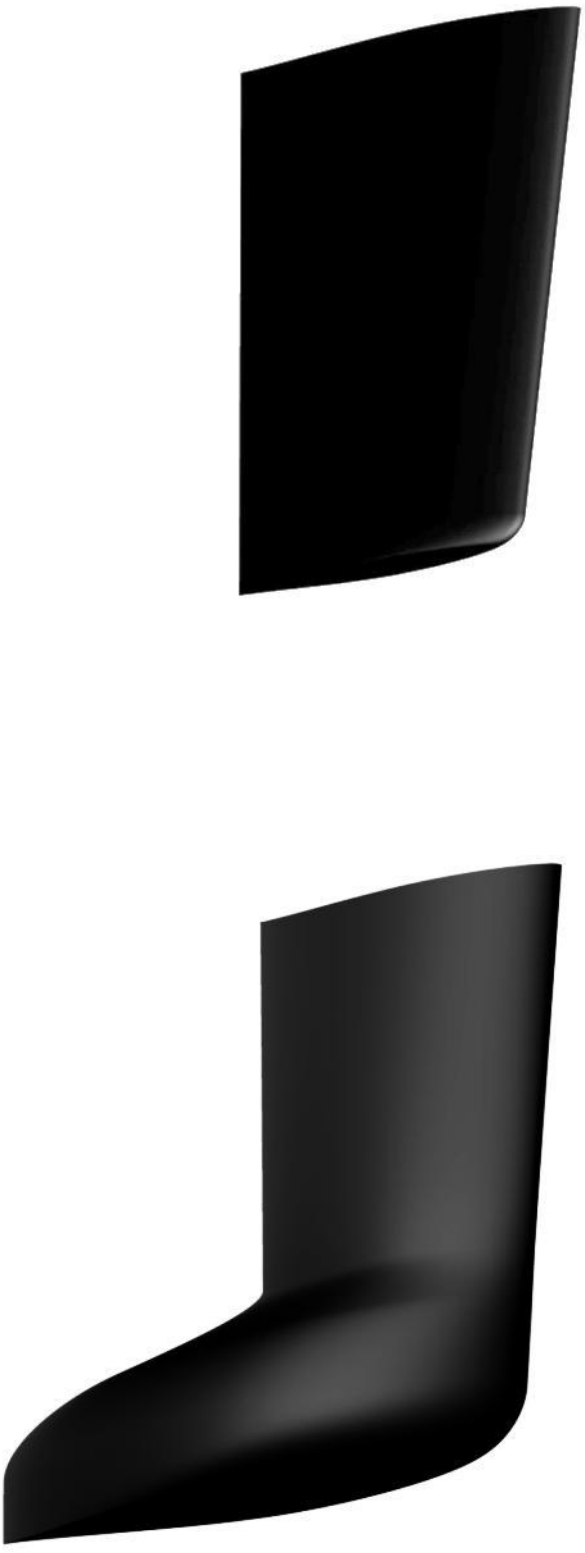

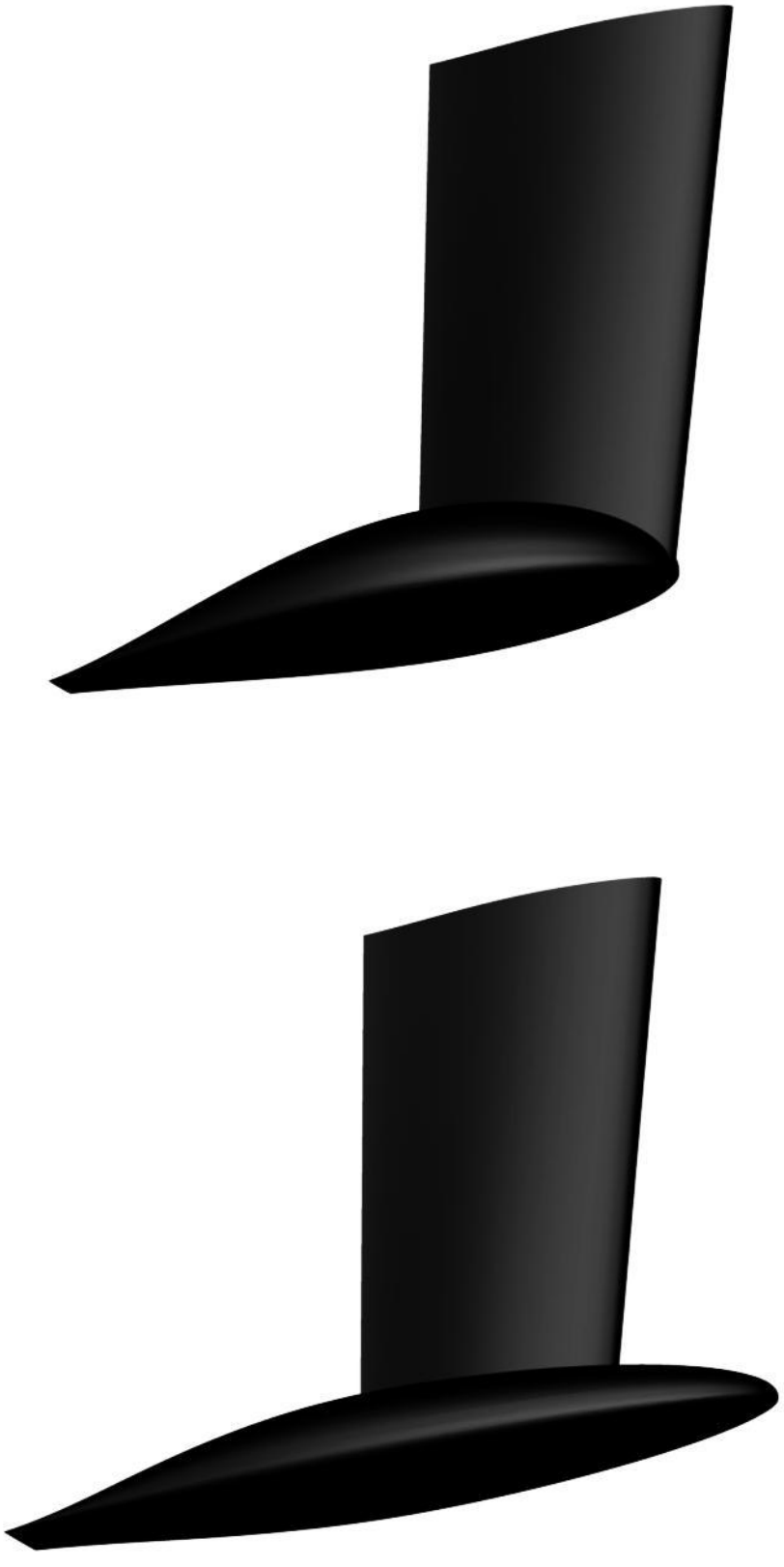

C: Mesh, perspective